The 13th Symposium on Polar Science

15 – 18 November 2022

National Institute of Polar Research
Research Organization of Information and Systems

Session OM

Polar Meteorology and Glaciology

Program and Abstracts

Conveners
Yutaka Tobo, and Shuji Fujita (NIPR)

【OM】Polar Meteorology and Glaciology

Scopes

This session covers research topics from the fields of atmospheric science, meteorology, glaciology, sea ice, oceanography, and paleoclimatology.

Conveners : **Yutaka Tobo, and Shuji Fujita (NIPR)**

Real-time Oral presentations (09:55 – 12:00, 13:30 – 15:10)

Date: Wed. 16 November

Chair: Tomotaka Saruya (NIPR)			
	9:55 - 10:00	Opening	Yutaka Tobo (NIPR)
OMo1	**10:00 - 10:20**	Improvement of the dielectric tensor measurement as a method to measure density, 3D porous structure and crystal orientation fabric of ice cores: realization of high spatial resolution measurement and its impacts	*Shuji Fujita (NIPR & SOKENDAI), Tomotaka Saruya (NIPR), Ryo Inoue (SOKENDAI)
OMo2	**10:20 - 10:40**	Development of crystal orientation fabric in the Dome Fuji ice core in East Antarctica: implications for the deformation regime in ice sheets	Tomotaka Saruya (NIPR), *Shuji Fujita (NIPR & SOKENDAI), Yoshinori Iizuka (ILTS), Atsushi Miyamoto (Hokkaido Univ.), Hiroshi Ohno (KIT), Akira Hori (KIT), Wataru Shigeyama (NIPR), Motohiro Hirabayashi (NIPR), Kumiko Goto-Azuma (NIPR & SOKENDAI)
OMo3	**10:40 - 11:00**	Dependence of the future mass loss of the Antarctic ice sheet on climate forcing and ice-shelf disintegration	*Ralf Greve (ILTS, Hokkaido University), Christopher Chambers (ILTS, Hokkaido University), Takashi Obase (AORI, The University of Tokyo), Fuyuki Saito (JAMSTEC), Wing-Le Chan (AORI, The University of Tokyo), Ayako Abe-Ouchi (AORI, The University of Tokyo)
Chair: Daisuke Goto (NIPR)			
OMo4	**11:00 - 11:20**	Assessing and projecting surface air temperature conditions required to sustain permafrost in Japan	*Tokuta Yokohata (NIES), Go Iwahana (University of Alaska, Fairbanks), Kazuyuki Saito (JAMSTEC), Noriko Ishizaki (NIES), Taiga Matsushita (University of Tsukuba), Tetsuo Sueyoshi (JAMSTEC)
OMo5	**11:20 - 11:40**	Fire Weather Conditions in the Arctic Region	*Hiroshi Hayasaka (Hokkaido University)
OMo6	**11:40 - 12:00**	Synoptic-timescale variability of Arctic aerosol in three reanalyses and its relationship to the atmospheric circulation in summer	*Akio Yamagami (MRI), Mizuo Kajino (MRI), Takashi Maki (MRI), Takahiro Toyoda (MRI)

Lunch

Chair: Naohiko Hirasawa (NIPR)			
OMo7	**13:30 - 13:50**	Assessment of the Changing Role of Lower Tropospheric Temperature and Water Vapor Advection under Arctic Amplification Using a Large-scale Ensemble Model Dataset	*Masatake Hori (AORI, The University of Tokyo), Masakazu Yoshimori (AORI, The University of Tokyo)
OMo8	**13:50 - 14:10**	The Detection and Distribution of Atmospheric Rivers in the South Polar Region	*Kazu Takahashi (Graduate School of Science, Kyoto University), Takatoshi Sakazaki (Graduate School of Scince, Kyoto University)

	14:10 - 15:10	3-minute poster appeal (17 short talks of OMp1 – OMp17)
	15:10 - 15:30	Break
	15:30 - 17:30	Poster session core time

Real-time Poster presentations (15:30 – 17:30)

Date: Wed. 16 November

OMp1	Improvement in thermodynamics computation in a numerical ice-sheet model IcIES	*Fuyuki Saito (JAMSTEC), Takashi Obase (AORI, The University of Tokyo), Ayako Abe-Ouchi (AORI, The University of Tokyo)
OMp2	Estimates of Antarctic ice sheet surface accumulation using camera images	*Konosuke Sugiura (University of Toyama), Naohiko Hirasawa (NIPR), Naoyuki Kurita (Nagoya University), Fumio Nakazawa (NIPR), Shun Tsutaki (NIPR), Kenji Kawamura (NIPR), Hiroshi Ohno (Kitami Institute of Technology), Shuji Fujita (NIPR), Ikumi Oyabu (NIPR), Takashi Yamanouchi (NIPR), Hideaki Motoyama (NIPR)
OMp3	Formation of layered firn within near-surface depths around Dome Fuji, East Antarctica from physical and chemical analyses of multiple firn cores	*Ryo Inoue (SOKENDAI & NIPR), Shuji Fujita (NIPR & SOKENDAI), Kenji Kawamura (NIPR & SOKENDAI, JAMSTEC), Motohiro Hirabayashi (NIPR), Kumiko Goto-Azuma (NIPR & SOKENDAI), Ikumi Oyabu (NIPR), Fumio Nakazawa (NIPR & SOKENDAI), Hideaki Motoyama (NIPR & SOKENDAI)
OMp4	The Dome Fuji ice core DF2021 chronology (0 – 207 kyr BP)	*Ikumi Oyabu (NIPR), Kenji Kawamura (NIPR), Christo Buizert (OSU), Frédéric Parrenin (IGE), Anais Orsi (LSCE), Kyotaro Kitamura (NIPR), Shuji Aoki (Tohoku University), Takakiyo Nakazawa (Tohoku Univeisity)
OMp5	Changes in flux, size and composition of dust at Dome Fuji, Antarctica across Termination I	*Kumiko Goto-Azuma (NIPR & SOKENDAI), Motohiro Hirabayashi (NIPR), Kaori Fukuda (NIPR), Jun Ogata (NIPR), Yoshimi Ogawa-Tsukagawa (NIPR), Kyotaro Kitamura (NIPR), Ayaka Yonekura (NIPR & SOKENDAI & Marine Works Japan), Shuji Fujita (NIPR & SOKENDAI), Kenji Kawamura (NIPR & SOKENDAI), Fumio Nakazawa (NIPR & SOKENDAI)
OMp6	Variations in mineralogy of dust in ice cores obtained from northwestern and northeastern Greenland over the past 100 years	*Naoko Nagatsuka (NIPR), Kumiko Goto-Azuma (NIPR & SOKENDAI), Akane Tsushima (Chiba University), Koji Fujita (Nagoya University), Sumito Matoba (ILTS), Yukihiko Onuma (JAXA), Yuki Komuro (LERMF), Motohiro Hirabayashi (NIPR), Jun Ogata (NIPR), Yoshimi Ogawa-Tsukagawa (NIPR), Kyotaro Kitamura (NIPR), Teruo Aoki (NIPR & SOKENDAI), Trevor James Popp (University of Copenhagen), Dorthe Dahl-Jensen (University of Copenhagen)
OMp7	Snow accumulation inferred from a GPR survey around the Southeastern Dome, Greenland Ice Sheet	*Masahiro Minowa (Hokkaido University), Koji Fujita (Nagoya University), Sumito Matoba (Hokkaido University), Yoshinori Iizuka (Hokkaido University)
OMp8	Monitoring of polar snow for 20 years by satellite microwave observations	*Riona Kasakawa (NIPR), Hiroyuki Enomoto (NIPR)

OMp9	Characteristics of cloud fraction and shortwave downward radiation at Syowa Station with ground-based observations	*Yumi Shimode (Nara Women's University), Mana Takada (Nara Women’s University), Amiri Yokotani (Nara Women’s University), Makoto Kuji (Nara Women's University), Masanori Yabuki (Kyoto University), Naohiko Hirasawa (NIPR & SOKENDAI)
OMp10	Comparison of cloud fractions from whole-sky camera observations around Syowa Station	Makoto Kuji (Nara Women's University), *Amiri Yokotani (Nara Women's University), Mana Takada (Nara Women's University), Yumi Shimode (Nara Women's University), Masanori Yabuki (Kyoto University), Naohiko Hirasawa (NIPR & SOKENDAI)
OMp11	4-year (2018-2021) variations of river surface temperature and channel width in the Arctic region derived from GCOM-C/SGLI	*Masahiro Hori (University of Toyama)
OMp12	A hemispheric extreme warm winter in 2019-20 enhanced by the highest sea surface temperature around mid-latitude	*Yuta Ando (Niigata University / National Institute of Technology, Suzuka College), Yoshihiro Tachibana (Weather and Climate Dynamics Division, Mie University)
OMp13	Seasonal variations of the partial pressure of CO_2 in surface water and quantitative assessment of its drivers in the Pacific Sector of the Arctic Ocean from winter to summer	*Manami Tozawa (Hokkaido University), Daiki Nomura (Hokkaido University), Mariko Hatta (JAMSTEC), Amane Fujiwara (JAMSTEC), Sayaka Yasunaka (Tohoku University), Akihiko Murata (JAMSTEC)
OMp14	Global distribution of decoupling between silicate and nitrate in the ocean	*Xianliang Pan (Hokkaido University), Xiangxing Lai (Hokkaido University), Bofeng Li (Hokkaido University), Yutaka Watanabe (Hokkaido University)
OMp15	Sea Ice Thickness Measurement Using UAV-SfM	*Yuki Ouchi (Kitami Institute of Technology), Kazutaka Tateyama (Kitami Institute of Technology), Tatsuya Watanabe (Kitami Institute of Technology), Kohei Sato (Civil Engineering Research Institute for Cold Region), Takuji Waseda (The University of Tokyo), Tsubasa Kodaira (The University of Tokyo), Ryosuke Uchiyama (The University of Tokyo)
OMp16	Lagged effect of tropical ocean on sea ice variability in the Sea of Okhotsk	*Mitsuki Takehata (Weather and Climate Dynamics Division, Mie University), Yoshihiro Tachibana (Weather and Climate Dynamics Division, Mie University), Yuta Ando (Niigata University & National Institute of Technology, Suzuka College)
OMp17	Seasonal and interannual changes in the lake surface of Izunuma wetland	*Tatsuru Sato (National Institute of Technology)

Improvement of the dielectric tensor measurement as a method to measure density, 3D porous structure and crystal orientation fabric of ice cores: realization of high spatial resolution measurement and its impacts

Shuji Fujita[1,2], Tomotaka Saruya[1] and Ryo Inoue[2]
[1]*NIPR*
[2]*SOKENDAI*

Major physical properties of ice cores include (i) densification from snow, firn to ice, and (ii) evolution of 3D porous structure composed of ice matrix and porous space. In addition, (iii) crystal orientation fabric (COF) is an important property to reveal degree of deformability (or viscosity) of polycrystalline ice. These three items are measurable with a method Dielectric Tensor Measurement (hereinafter, DTM) for which we use millimeter wave open resonators (Fujita et al. 2009, 2016, Saruya et al., 2021, 2022). The method has many advantageous conditions: (i) non-destructive, (ii) high-spatial resolution (a cylinder volume with ~15mm in diameter), (iii) continuous, (iv) rapid, and (v) safe. The authors have developed the DTM method of ice core analyses for the tentorial values of relative permittivity. We established a system to measure thick sections with thickness range from 5 mm to 70 mm with a diameter of about 15 mm, by a new design of the open resonator. In addition, based on this improvement, we realized common use of samples for DTM and Continuous Flow Analysis (CFA); CFA is the modern and major analytical method for ice cores to analyze major elements, water stable isotope ratio, dusts, gas components and so on with high-spatial resolution, continuously and rapidly. For measurements on density, anisotropy of the 3D porous structure, or crystal orientation fabrics, we can acquire basic physical property information of ice cores very efficiently compared with any conventional methods for these. In addition, because sample sticks can be common with CFA, we can reduce both ice core consumption and preparation work (cutting, microtoming and/or ice core management work). Because both CFA and the DTM use common ice samples, we can maximize information extraction from precious ice cores, making synergistic effects between multiple kinds of data. The DTM can be one of routine methods for future studies of ice cores. We can enhance better understanding the physical structures and deformation regimes within polar ice sheets and glaciers.

References

Fujita, S, Okuyama, J, Hori, A and Hondoh, T (2009) Metamorphism of stratified firn at Dome Fuji, Antarctica: a mechanism for local insolation modulation of gas transport conditions during bubble close off. J. Geophys. Res. 114, F03023. doi: 10.1029/2008jf001143

Fujita, S.et al. (2016). Densification of layered firn in the ice sheet at Dome Fuji, Antarctica. J. Glaciol., 62(231), 103-123. doi:10.1017/jog.2016.16

Saruya, T., Fujita, S., & Inoue, R. (2022). Dielectric anisotropy as indicator of crystal orientation fabric in Dome Fuji ice core: Method and initial results. J. Glaciol., 68(267), 65-76. doi:10.1017/jog.2021.73

Saruya, T., Fujita, S., Iizuka, Y., Miyamoto, A., Ohno, H., Hori, A., Shigeyama, W., Hirabayashi, M., and Goto-Azuma, K.: Development of crystal orientation fabric in the Dome Fuji ice core in East Antarctica: implications for the deformation regime in ice sheets, The Cryosphere, 16, 2985–3003, https://doi.org/10.5194/tc-16-2985-2022, 2022.

Development of crystal orientation fabric in the Dome Fuji ice core in East Antarctica: implications for the deformation regime in ice sheets

Tomotaka Saruya[1], Shuji Fujita[1,2,*], Yoshinori Iizuka[3], Atsushi Miyamoto[4], Hiroshi Ohno[5], Akira Hori[5], Wataru Shigeyama[1], Motohiro Hirabayashi[1] and Kumiko Goto-Azuma[1,2]

[1]*NIPR,* [2]*SOKENDAI,* [3]*ILTS, Hokkaudo Univ.,* [4]*Institute for the Advancement of Higher Education, Hokkaudo Univ.,* [5]*KIT,*

The crystal orientation fabric (COF) of a polar ice sheet has a significant effect on the rheology of the sheet. With the aim of better understanding the deformation regime of ice sheets, the present work investigated the COF in the upper 80% of the depth within the 3035 m long Dome Fuji Station ice core drilled at one of the dome summits in East Antarctica. Dielectric anisotropy (Δε) data were acquired as a novel indicator of the vertical clustering of COF resulting from vertical compressional strain within the dome, at which the ice cover has an age of approximately 300 kyrs BP. The Δε values were found to exhibit a general increase moving in the depth direction, but with fluctuations over distances on the order of 10-102 m. In addition, significant decreases in Δεe were found to be associated with depths corresponding to three major glacial to interglacial transitions. These changes in Δε are ascribed to variations in the deformational history caused by dislocation motion occurring from near-surface depths to deeper layers. Fluctuations in Δε over distances of less than 0.5 m exhibited a strong inverse correlation with Δε at depths greater than approximately 1200 m, indicating that they were enhanced during the glacial/interglacial transitions. The Δε data also exhibited a positive correlation with the concentration of chloride ions together with an inverse correlation with the amount of dust particles in the ice core at greater depths corresponding to decreases in the degree of c-axis clustering. Finally, we found that fluctuations in Δε persisted to approximately 80% of the total depth of the ice sheet. These data suggest that the factors determining the deformation of ice include the concentration of chloride ions and amount of dust particles, and that the layered contrast associated with the COF is preserved all the way from the near-surface to a depth corresponding to approximately 80% of the thickness of the ice sheet. These findings provide important implications regarding further development of the COF under the various stress-strain configurations that the ice will experience in the deepest region, approximately 20% of the total depth from the ice/bed interface.

References

Saruya, T., Fujita, S., & Inoue, R. (2022). Dielectric anisotropy as indicator of crystal orientation fabric in Dome Fuji ice core: Method and initial results. J. Glaciol., 68(267), 65-76. doi:10.1017/jog.2021.73

Saruya, T., Fujita, S., Iizuka, Y., Miyamoto, A., Ohno, H., Hori, A., Shigeyama, W., Hirabayashi, M., and Goto-Azuma, K.: Development of crystal orientation fabric in the Dome Fuji ice core in East Antarctica: implications for the deformation regime in ice sheets, The Cryosphere, 16, 2985–3003, https://doi.org/10.5194/tc-16-2985-2022, 2022.

* Shuji Fujita: Presenter

Dependence of the future mass loss of the Antarctic ice sheet on climate forcing and ice-shelf disintegration

Ralf Greve[1,2], Christopher Chambers[1], Takashi Obase[3], Fuyuki Saito[4], Wing-Le Chan[3], Ayako Abe-Ouchi[3]

[1]*Institute of Low Temperature Science, Hokkaido University, Sapporo, Japan*

[2]*Arctic Research Center, Hokkaido University, Sapporo, Japan*

[3]*Atmosphere and Ocean Research Institute, The University of Tokyo, Kashiwa, Japan*

[4]*Japan Agency for Marine-Earth Science and Technology, Yokohama, Japan*

As part of the Coupled Model Intercomparison Project Phase 6 (CMIP6), the Ice Sheet Model Intercomparison Project for CMIP6 (ISMIP6) was devised to assess the likely sea-level-rise contribution from the Antarctic and Greenland ice sheets until the year 2100. ISMIP6 used future climate scenarios as forcings for ice-sheet models developed by several international groups. Results obtained for the Antarctic ice sheet are described by Seroussi et al. (2020) and Payne et al. (2021).

Extended projections for the Antarctic ice sheet until the year 2300 have been devised to investigate the longer-term response of the ice sheet ("ISMIP6 2300 Antarctica", tinyurl.com/ismip6-ais-2300). The suite of experiments contains 14 experiments, 12 of which are for RCP8.5/SSP5-8.5 and 2 for RCP2.6/SSP1-2.6. We carried out these experiments with the ice-sheet model SICOPOLIS (www.sicopolis.net) and the same set-up as used for the original ISMIP6 experiments (Greve et al., 2020). Results are shown in Figure 1. For the control run with a constant, 1995–2014 average climate, the ice sheet is stable until the year 2300. For RCP8.5/SSP5-8.5, it suffers a severe mass loss, which amounts to ~3.1 m SLE (sea-level equivalent) for the 12-experiment mean, and > 5 m SLE for the most sensitive experiment. Most of this loss originates from West Antarctica. Ice-shelf collapse due to surface melting, parameterized explicitly in four of the experiments, increases the mass loss significantly. By contrast, the mass loss is below average for the four experiments in which the last-21st-century climate is merely repeated into the future without any further trend. For RCP2.6/SSP1-2.6, the loss is limited to a two-experiment mean of ~0.11 m SLE, demonstrating the potential of climate-change mitigation for limiting the decay of the ice sheet.

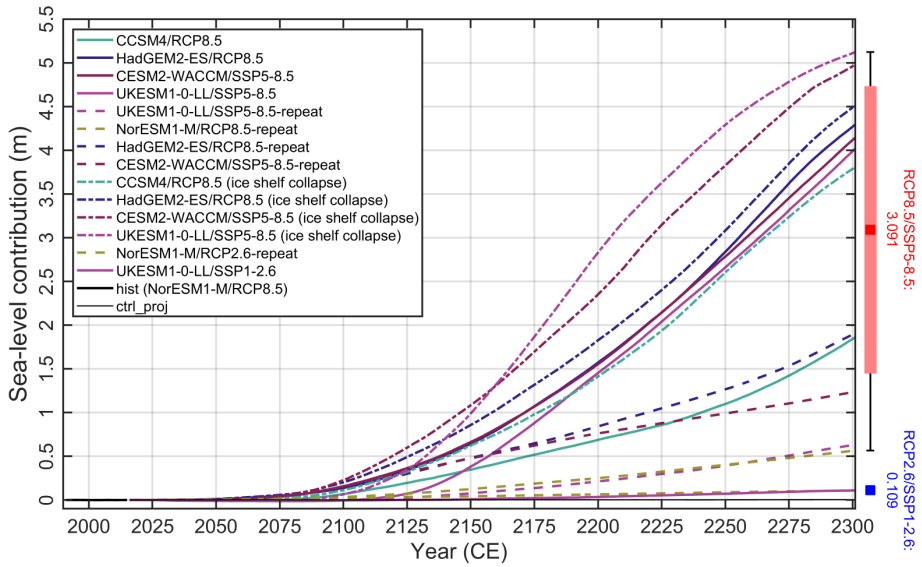

Figure 1. Historical run (hist), projection control run (ctrl_proj) and future climate experiments until the year 2300: Simulated ice mass change, counted positively for loss and expressed as sea-level contribution. The red and blue boxes to the right show the means for RCP8.5/SSP5-8.5 and RCP2.6/SSP1-2.6, respectively (RCP8.5/SSP5-8.5: also ± 1-sigma); the whiskers show the corresponding full ranges.

References

Greve, R., R. Calov, T. Obase, F. Saito, S. Tsutaki and A. Abe-Ouchi. 2020. ISMIP6 future projections for the Antarctic ice sheet with the model SICOPOLIS. Technical report, Zenodo, doi: 10.5281/zenodo.3971232.

Seroussi, H. and 46 others. 2020. ISMIP6 Antarctica: a multi-model ensemble of the Antarctic ice sheet evolution over the 21st century. Cryosphere, 14 (9), 3033-3070, doi: 10.5194/tc-14-3033-2020.

Payne, A. J. and 63 others. 2021. Future sea level change under Coupled Model Intercomparison Project Phase 5 and Phase 6 scenarios from the Greenland and Antarctic ice sheets. Geophys. Res, Lett., 48 (16), e2020GL091741, doi: 10.1029/2020GL091741.

Assessing and projecting surface air temperature conditions required to sustain permafrost in Japan

Tokuta Yokohata[1], Go Iwahana[2], Kazuyuki Saito[3], Noriko N. Ishizaki[1], Taiga Matsushita[4], and Tetsuo Sueyoshi[3]

[1]*National Institute for Environmental Studies*

[2]*University of Alaska, Fairbanks*

[3]*Japan Agency for Marine-Earth Science and Technology*

[4]*University of Tsukuba*

Permafrost covers a wide area of the Northern Hemisphere, including high-altitude mountainous areas and even at mid-latitudes. There is concern that the thawing of mountain permafrost can cause slope instability and substantially impact alpine ecosystems, and because permafrost in mountainous areas is difficult to observe, detailed analyses have not been performed on its current distribution and future changes. Although previous studies have observed permafrost only at a limited number of points in Japan (e.g., Daisetsu Mountains, Mt. Fuji, and Mt. Tateyama in the Northern Japan Alps), we show that permafrost potentially exists in nine domains in Japan (Daisetsu Mountains, Mt. Fuji, Northern and Southern Japan Alps, Hidaka Mountains, Mt. Shiretoko, Sharidake, Akandake, and Yotei). In the Daisetsu Mountains and Mt. Fuji, the environmental conditions required for maintaining at least some permafrost are projected to remain in the future if a decarbonized society is achieved (RCP2.6 or RCP4.5). However, if greenhouse gas emissions continue to increase (RCP8.5), the environmental conditions required for sustaining permafrost are projected to disappear in the second half of the 21st century. In other domains, the environmental conditions required for maintaining permafrost are either projected to disappear in the next ten years (Hidaka Mountains, Northern Japan Alps) or they have almost disappeared already (Southern Japan Alps, Mt. Shiretoko, Sharidake, Akandake, and Yotei). Our projections show that climate change has a tremendous impact on Japan's mountain permafrost environment and suggests the importance of monitoring the mountain environment and considering measures for adapting to future climate change.

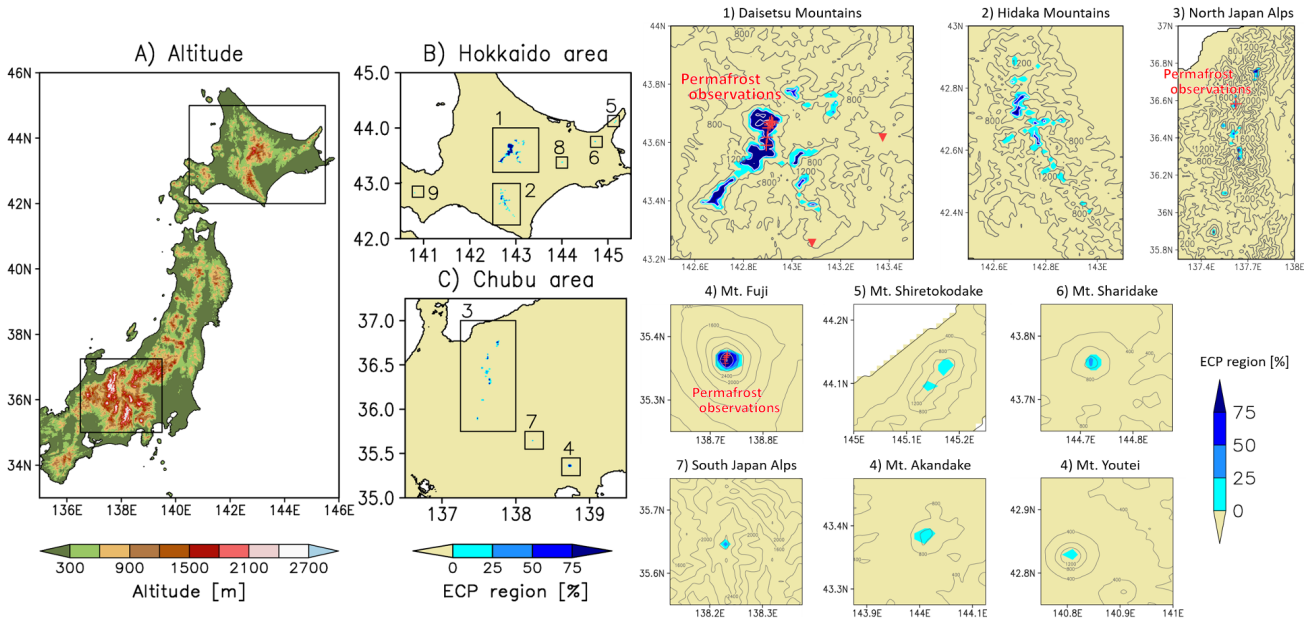

Figure 1. **Left**: A) Map showing the altitude [m] of northern and eastern Japan, and the distribution of regions with surface air temperatures that favor the maintenance of permafrost (the Environmentally Conditioned Permafrost regions) in Japan; B) Hokkaido and C) the Chubu. The numbers indicate (1) Daisetsu Mountains, (2) Hidaka Mountains, (3) Northern Japan Alps, (4) Mt. Fuji, (5) Mt. Shiretoko, (6) Mt. Shari, (7) Southern Japan Alps, (8) Mt. Akandake, and (9) Mt. Yotei. **Right**: Environmentally Conditioned Permafrost regions in Japan under the current climate conditions (averaged over 1999–2018). The distribution of the environmentally conditioned permafrost region is based on probabilities estimated by nine bias-corrected climate scenarios. Red points indicate sites where permafrost has been observed. The observations of sporadic permafrost in Shikaribetsu and Oketo are shown as ▼, and other observations are shown as + . The contour interval is 400 m

References

Yokohata T. et al. (2022) Assessing and projecting surface air temperature conditions required to sustain permafrost in Japan, Progress in Earth and Planetary Science 9, 30. https://doi.org/10.1186/s40645-022-00498-z

Fire Weather Conditions in the Arctic Region

Hiroshi Hayasaka
Arctic Research Center, Hokkaido University

Fire activity in 288 areas (2.5° N × 10° E) in the Arctic region (50°–70° N, 0°–360° E) was analyzed using satellite hotspot data (number of HSs = about 4.4 million) from 2002 to 2021. A total of 21 high fire density areas were selected and their fire–weather conditions during each active fire period were analyzed using weather and temperature maps at upper and lower air (over 1820 maps in all). Analysis results of fire–weather conditions for high fire density areas in the Arctic region (North Eurasia and North America) are summarized in the below.

Active fires in central and eastern Siberia started by LWM (large westerly meandering) caused by COL detached from Arctic low-pressure systems over the continent (west and central Siberia). Very active fires on HS peak days in central and eastern Siberia occurred under COH detached from a ridge extending from the Tibet plateau and Arabia. In North America, active fires also started by LWM caused by COL detached from Arctic low- pressure systems over the Bering Sea and the Gulf of Alaska. However, fires were not so active until high-pressure systems (COH and ridge) extended from the Great Basin. Analysis results may suggest there are six major fire regimes in the Arctic region: (1) Eastern Europe, (2) Central and East Siberia (Sakha), (3) Far east high-latitude Siberia (northern Sakha), (4) Far east low-latitude Siberia (southern Khabarovsk), (5) Alaska, and (6) Western Canada.

Lastly, we should prepare for the next large-scale fires due to climate change by applying the fire–weather analysis approach described in this paper. Since we can predict occurrence of active fires, we could prevent active fires by making fire breaks, prescribed fires, and so on. Our fight against wildland fires is one of the executable ways to mitigate global warming.

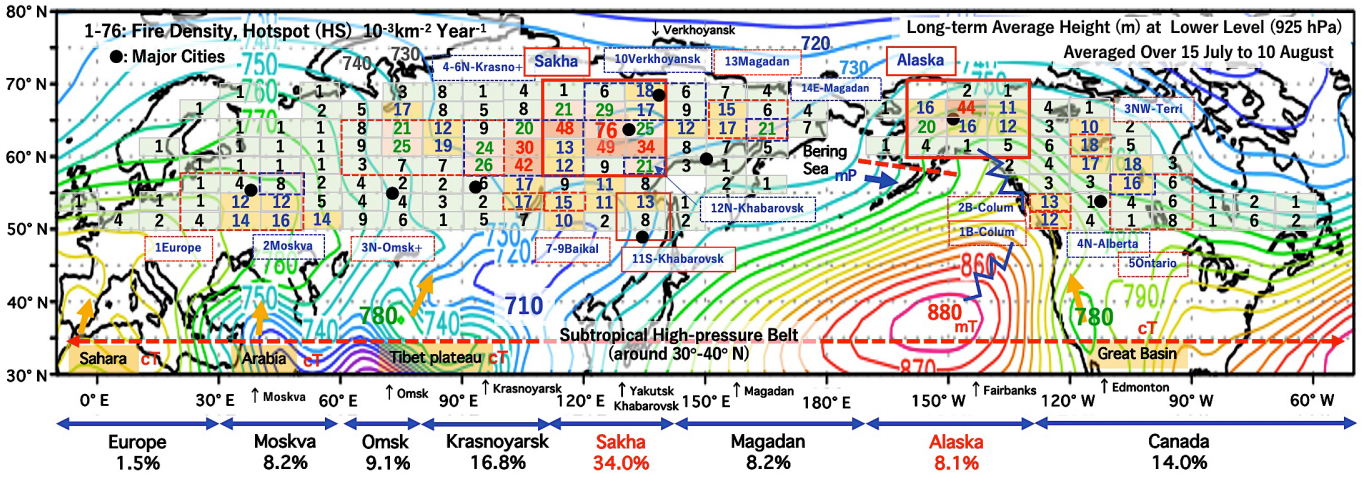

Figure 1. Map of part of the northern hemisphere (30°–80° N, -10°–310° E). The Arctic study region (50°–70° N, 0°–360° E) was divided into 288 areas (2.5° N × 10° E), showing their fire density (hotspot (HS) 10^{-3} km^{-2} Year^{-1}). The fire density of each cell is indicated by the numbers 1 to 75 (smaller than 1 is not shown). Eight wide area names by longitude (20°–80° E)) are shown at the bottom of the figure such as “Europe”, “Moskva”, etc. Two rectangles with a red solid line show two major study regions of Sakha and Alaska. Rectangles with a red or blue dotted line show other study areas and their names are found near them, such as “3N-Omsk+”. Major cities are indicated by black circles and their names are shown at the bottom of the figure. The base map is the lower air (925 hPa) weather map (long-term average map for 74 years from 1948) obtained from the NCEP/NCAR 40-year reanalysis data.

References

Hayasaka, H.; Tanaka, H.L.; Bieniek, P.A. Synoptic-scale fire weather conditions in Alaska. Polar Sci. 2016, 10, 217–226. https://doi.org/10.1016/j.polar.2016.05.001.

Hayasaka, H.; Yamazaki, K.; Naito, D. Weather conditions and warm air masses in southern Sakha during active wildfire periods. J. Disaster Res. 2019, 14, 641–648. https://doi.org/10.20965/jdr.2019.p0641.

Hayasaka, H.; Yamazaki, K.; Naito, D. Weather Conditions and Warm Air Masses during Active Fire-periods in Boreal Forests. Polar Sci. 2019, 22, 100472. https://doi.org/10.1016/j.polar.2019.07.002.

Hayasaka, H. Rare and Extreme Wildland Fire in Sakha in 2021. Atmosphere 2021, 12, 1572. https://doi.org/10.3390/atmos12121572.

Synoptic-timescale variability of Arctic aerosol in three reanalyses and its relationship to the atmospheric circulation in summer

Akio Yamagami[1], Mizuo Kajino[1,2], Takashi Maki[1], and Takahiro Toyoda[1]
[1]*Meteorological Research Institute (MRI), Japan Meteorological Agency (JMA), Tukuba*
[2]*Faculty of Life and Environmental Sciences, University of Tsukuba, Tsukuba*

The Arctic has warmed faster than the global average. Atmospheric aerosols can change the radiation budget through aerosol–radiation interaction, aerosol-cloud interaction, and decreasing surface albedo over snow and sea ice. Hence, aerosol influence is considered one of the most important factors for the Arctic climate system. Still, the estimation of Arctic aerosol effects contains large uncertainties. Although several observational campaigns have been conducted, the sparse observation network over the Arctic is one of the reasons for the uncertainties. Aerosol reanalyses, which fill the gap between observations through model dynamics, provide spatiotemporal distributions over the globe. Recently, Xian et al. (2022) showed that three aerosol reanalyses generally reproduce the monthly climatological variabilities, and negative (positive) trends in spring (summer) of aerosol optical depth (AOD) over the Arctic as estimated from satellite observations. However, no study has yet investigated the relationship between Arctic aerosol behaviors and synoptic disturbances in summer, when Arctic cyclones (ACs) are most frequently observed.

In this study, we assessed the Arctic AOD variability in three reanalyses (JRAero, CAMSRA, and MERRA2) and investigated its relationship to synoptic-scale atmospheric circulation. In all the Arctic regions, except in the North Atlantic, the AOD becomes highest in July–August. The temporal variabilities (average, median, and quartile values) (Fig. 1a) and horizontal distribution of total AOD in summer were generally consistent among the three reanalyses. In contrast, the contributions of individual aerosol species to the total AOD are quite different among the reanalyses (Fig. 1b-f). The first and second largest contributions to the total AOD were organic carbon and sulfate in all reanalyses, but the sea salt contribution was comparable to the sulfate contribution in JRAero. Compared to the limited satellite observations, the summertime AOD variability is generally represented in all reanalyses (R>0.6), albeit its magnitude exhibited an error as large as the average AOD (RMSE was equal to the average). The EOF analysis showed large variabilities over Northern Eurasia on the synoptic timescales. Our results highlighted that the essential role of the generation and development of summertime Arctic cyclones and the associated moisture and precipitation in aerosol transportation and deposition over the Arctic (Fig. 2).

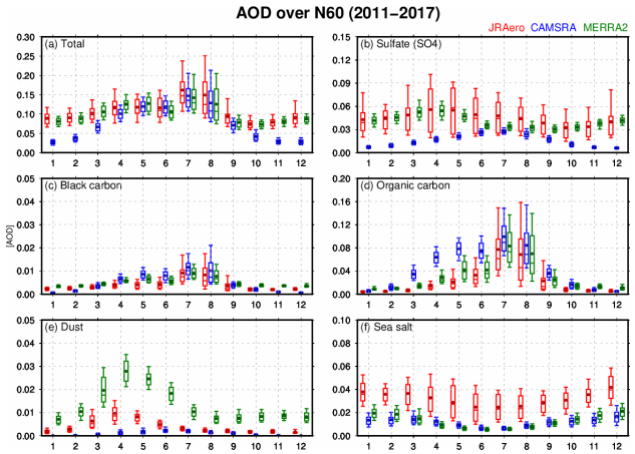

Figure 1. (a) Histogram of the six-hourly total AOD and the contributions of (b) sulfate, (c) black carbon, (d) organic carbon, (e) dust, and (f) sea salt aerosol to the total AOD in JRAero (red), CAMSRA (blue), and MERRA-2 (green) over north of 60ºN.

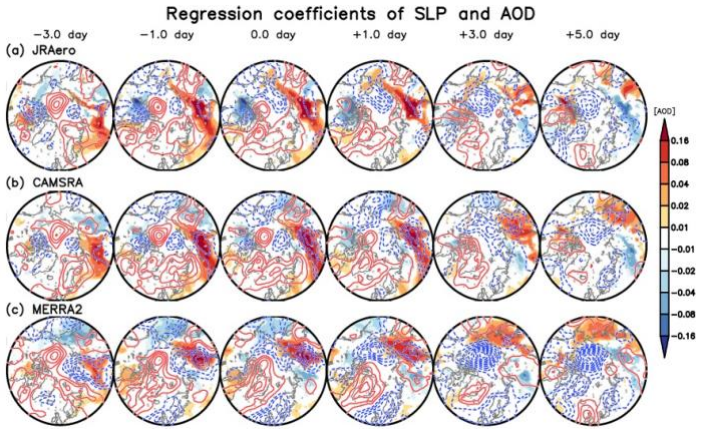

Figure 2. Total AOD (shading) regressed onto PC-1in (a) JRAero, (b) CAMSRA, and (c) MERRA2 from the −3 to +5-day lag. The blue (positive) and red (negative) contours show the SLP in JRA-55 regressed onto EOF-1 for each aerosol reanalysis.

References

Xian, P., Zhang, J. et al., Arctic spring and summertime aerosol optical depth baseline from long-term observations and model reanalyses – Part 1: Climatology and trend. Atmospheric Chemistry and Physics, 22(15), 9915–9947, 2022.

Acknowledgments

This study was mainly supported by the Japanese Society for the Promotion of Sciences (JSPS) KAKENHI grant no. JP22J01703, and partly supported by the Arctic Challenge for Sustainability II (ArCS II), Grant Number JPMXD1420318865.

Assessment of the Changing Role of Lower Tropospheric Temperature and Water Vapor Advection under Arctic Amplification Using a Large-scale Ensemble Model Dataset

Masatake E. Hori[1] and Masakazu Yoshimori[1]
[1]*Atmosphere and Ocean Research Institute, The University of Tokyo, Kashiwa, Japan*

The near-surface temperature over the Arctic experiences an increased amount of warming compared to the global average under the elevated concentration of greenhouse gases in a phenomenon known as the Arctic Amplification (AA). One of the leading topics of debate concerning the AA is the relative importance of locally driven feedback such as ice albedo feedback against the remote transport of heat into the Arctic from the mid-latitudes via the advection of temperature and water-vapor. While many studies emphasize the importance of locally driven processes such as sea-ice reduction and change in radiative feedbacks, studies such as Clark et al. (2021) points out that horizontal temperature advection driven by large-scale atmospheric patterns also plays a role in maintaining the AA.

In this study, we further investigate the role of temperature advection in the lower troposphere under changing level of global warming. We use the Database for Policy Decision-Making for Future Climate Change (d4PDF; Mizuta et al. 2017) which is a large ensemble AGCM dataset designed to quantify the response in atmospheric processes under changing state of greenhouse gasses and sea surface temperature as well as sea-ice boundaries. Using the 30-year climatology of the non-warming simulation (HPB-NAT) as a reference, the difference in temperature advection under changing basic states of the historical experiment (HPB) and 2K and 4K warming experiments (HFB-2K and 4K) is examined. Here, we use the modified formulation of Wang et al. (2019) to decompose the temperature and moisture advection into components relative to dynamical changes and thermodynamical changes under global warming. The formulation allows to quantify the contribution of changes in the mean state of the wind and the temperature/moisture field under difference simulations.

Applying this method to the temperature in the lower tropospheric level of 925hPa, it is found that under the HPB experiment, the total change in temperature advection is overall positive in the Arctic driven by a stronger dynamical component of advection along the sea-ice boundary in the North Atlantic and the Northern coastline of the Eurasian continent. However, this feature drastically changes under elevated global warming experiments of HFB-2K and HFB-4K where the thermodynamical component of advection turns negative due to weaker temperature gradient. The contribution of the eddy term which is related to the effect of sub-monthly transient eddies dissipating the heat released from the ocean also turns negative and dominates in the region where sea ice retreats in comparison to the HPB-NAT experiment. Taking an average over the Arctic, the total role of atmospheric advection in the lower troposphere turns negative under the HFB-2K and HFB-4K experiments. Reduction in sea ice along the Eurasian continent leads to larger sensible heat released in the region which is dissipated by the transient eddies. From an atmospheric advection point of view, this leads to a more negative signal in the eddy term which overcomes the effect of a stronger dynamical component in horizontal temperature advection under elevated global warming.

Further analysis is made focusing on the water vapor advection and its role under the changing basic state of wind and specific humidity. Increase in water vapor advection driven by the dynamical component is evident along the North Atlantic for HPB / HFB-2K / HFB-4K experiments which agrees with the positive Arctic Oscillation pattern in the models. In our presentation, we will further explore the role of water vapor advection in driving the regional lower tropospheric moistening including the seasonality and regional variability.

References

Clark J. P., V. Shenoy, S. B. Feldstein et al., The Role of Horizontal Temperature Advection in Arctic Amplification, J. Clim 34, 2957–2976, 2021

Mizuta R, A. Murata, M. Ishii et al, Over 5,000 Years of Ensemble Future Climate Simulations by 60-km Global and 20-km Regional Atmospheric Models, Bull Am Meteorol Soc 98, 1383–1398, 2017

Wang F, S. J. Vavrus, J. A. Francis, J. E. Martin, The role of horizontal thermal advection in regulating wintertime mean and extreme temperatures over interior North America during the past and future, Clim. Dyn. 53, 6125–6144, 2019

The Detection and Distribution of Atmospheric Rivers in the South Polar Region

Kazu Takahashi[1], Takatoshi Sakazaki[1]
[1]*Graduate School of Science, Kyoto University*

Atmospheric River (AR), is defined as a narrow, filamentary structure of water vapor flux, playing a significant role in moisture transport from mid to high latitude regions. In this study, we will focus on AR in the south polar region which are considered to be related with extreme snow accumulation events (Gorodetskaya et al., 2014) and even with the Antarctic Ice Sheet discharge (Wille et al., 2019). It should be noted that the geographical distribution of AR occurrence has yet to be examined in detail, while it may be important for understanding the zonally asymmetric changes of Antarctic ice sheet (Wingham et al., 2006).

In many previous studies, AR is defined as an event in which water vapor flux exceeds some threshold as determined at each grid point from long-term record. Such AR detection method, however, is not suitable for examining the geographical distribution of AR since AR is more difficult (easier) to detect in the region where AR tend to appear more (less) frequently. In this study, we use a method using a threshold based on the anomaly from zonal mean at each time step for the vertical integrated water vapor flux (IVT) (Zhu and Newell., 1998). That is, the threshold is common for all grids (on a particular latitude band at one time) so that the zonally asymmetric distribution can be detected. With this procedure, we aim at revealing the regional features of AR activity including their underlying mechanism.

The data set we used is the Japanese 55-year Reanalysis (JRA-55) data (Kobayashi et al., 2015), which provides global, 6-hourly atmospheric fields with a longitude-latitude resolution of 1.25° × 1.25° . Data over seven years between 2013 and 2019 are analyzed. The AR detection is based on IVT that is calculated with specific humidity and horizontal winds at 17 pressure levels from surface to 300hPa. First, some AR-like objects are detected in the case that the zonal anomaly of IVT has values above the maximum zonal anomaly multiplied by a factor of 0.3. These objects may have not only filamentary structures, but also spiral structures like a tropical cyclone. So, only the objects whose length is longer than 2000km and whose aspect ratio exceeds 2 are finally defined as AR. We investigate the geographical distribution of AR occurrence and AR-related meridional moisture transport (MMT) including their seasonal variations.

Figure 1a and 1b show the horizontal distribution of AR frequency and AR-related MMT, respectively. We find that the AR frequency has a zonally asymmetric structure around the Antarctica (Figure. 1 (a)). Between 40° S to 50° S, ARs appear more frequently in the Eastern Hemisphere than in the Western Hemisphere, while they tend to occur more frequently in the Western Hemisphere for the region southward of 50° S including the Antarctica. AR occurs only less than 10 days per year on the east Antarctica. Such geographical dependency has never been reported in previous studies as far as the authors know. The distribution of AR-related MMT is similar to that of AR frequency: large (small) moisture transport is observed in high (low) AR-frequency area (Figure. 1 (b)).

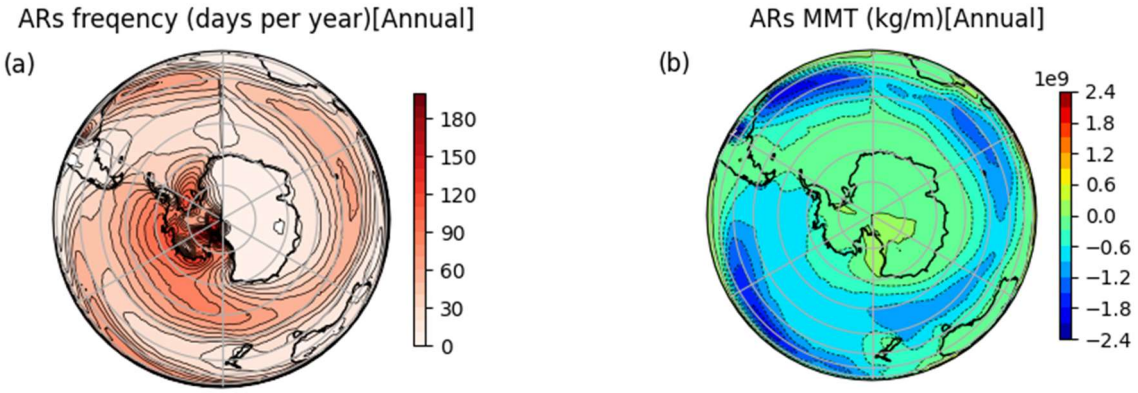

Figure 1. (a)Annual frequency of ARs and (b)Annual ARs-related meridional moisture transport (units: kg/m, poleward values are negative) in southern hemisphere for the years 2013-2019. ARs = Atmospheric rivers

The zonally asymmetric AR activity is likely related to the geographical pattern of storm tracks and the zonal jet streams in the Southern Hemisphere. In fact, the annual-mean eddy kinetic energy and zonal wind at 500 hPa have zonally asymmetric structures similar to the AR frequency distribution. The AR frequency shows a marked seasonal variation with maxima twice in

April and September; this seasonality is also found in zonal-mean zonal wind at 60° S. The observed geographical dependency of AR activity might be a key for understanding the zonal asymmetry in Antarctic Ice Sheet discharge because high frequency area of AR occurrence is corresponding to the area where ice sheet significantly discharges in the west Antarctica (Wingham et al., 2006).

References

Gorodetskaya, I. V., Tsukernik, M., Claes, K., Ralph, M. F., Neff, W. D., and Van Lipzig, N. P. M. (2014). The role of atmospheric rivers in anomalous snow accumulation in East Antarctica, Geophysical Research Letters, 41(17), 6199-6206.

Wille, J. D., Favier, V., Dufour, A., Gorodetskaya, I. V., Turner, J., Agosta, C., and Codron, F. (2019). West Antarctic surface melt triggered by atmospheric rivers, Nature Geoscience, 12(11), 911-916.

Wingham, D. J., Shepherd, A., Muir, A., and Marshall, G. J. (2006). Mass balance of the Antarctic ice sheet, Philos. T. A. Math. Phys. Eng. Sci., 364, 1627–1635.

Zhu, Y., and Newell, R. E. (1998). A proposed algorithm for moisture fluxes from atmospheric rivers. Monthly Weather Review, 126(3), 725-735.

Kobayashi, S., Ota, Y., Harada, Y., Ebita, A., Moriya, M., Onoda, H., Onogi, K., Kamahori, H., Kobayashi, C., Endo, H., Miyaoka, K., and Takahashi, K. (2015). The JRA-55 Reanalysis: General Specifications and Basic Characteristics, J. Meteorol. Soc. Jpn., 93, 5-48.

Improvement in thermodynamics computation in a numerical ice-sheet model IcIES

SAITO Fuyuki[1], Takashi OBASE[2], Ayako ABE-OUCHI[2]
[1]*Japan Agency for Marine-Earth Science and Technology*
[2]*Atmosphere and Ocean Research Institute, Univ. of Tokyo*

Computation of temperature field by numerical ice-sheet models is a key issue, in particular, for long-term and large-scale ice-sheet simulation. The velocity fields depend on the ice temperature field, because it determines the softness of the ice, and because the basal temperature determines the ice sliding condition. On the other hand, the evolution of temperature is affected by advection and strain-heating, which are function of those ice velocity and softness. These feedbacks may sometimes induce oscillation and/or instability. Many ice-sheet modeling studies have reported such characteristic features of ice-sheet dynamics, however, there still remain uncertainties to decide what is robust and what is not. Improvement in computation of temperature is one of the current major subjects on development of a numerical ice-sheet model IcIES. Toward this goal, (a) introduction of a higher-order numerical advection scheme (b) introduction of the enthalpy scheme to replace the current temperature equation are set as present development tasks in IcIES. The present study will report the progress in development of the two subjects and will show some demonstration how they affect the simulated temperature and ice-sheet evolution.

Estimates of Antarctic ice sheet surface accumulation using camera images

Konosuke Sugiura[1], Naohiko Hirasawa[2], Naoyuki Kurita[3], Fumio Nakazawa[2], Shun Tsukaki[2], Kenji Kawamura[2], Hiroshi Ohno[4], Shuji Fujita[2], Ikumi Oyabu[2], Takashi Yamanouchi[2] and Hideaki Motoyama[2]

[1]*University of Toyama*

[2]*National Institute of Polar Research*

[3]*Nagoya University*

[4]*Kitami Institute of Technology*

Snow depth measurements from Syowa Station to Dome Fuji using snow stakes at 2 km intervals (e.g., Motoyama et al., 2015) and automatic weather stations (AWS) at four points have been carried out by the Japanese Antarctic Research Expedition as part of a monitoring program for assessing the surface mass balance of the ice sheet. To obtain the daily data for snow surface conditions along a latitudinal transect from the coast to the inland, we have installed digital cameras at four stationary observation points (#1 H180, #2 Mizuho Station, #3 Relay Point, and #4 Dome Fuji. Fig.1) near the traverse routes on November 15, November 23, December 2 and December 13, 2017, respectively (Sugiura et al., 2019).

In this study, the snow depth was estimated from the camera images automatically taken of a red-white pole on the ice sheet. Comparison of snow depths with previous studies using snow stakes (Motoyama et al., 2015) showed that the values were within an approximately reasonable range. We will also compare these snow depth data with AWS-derived snow depth data and discuss some of the problems with the observations.

Figure 1. Stationary observation points.

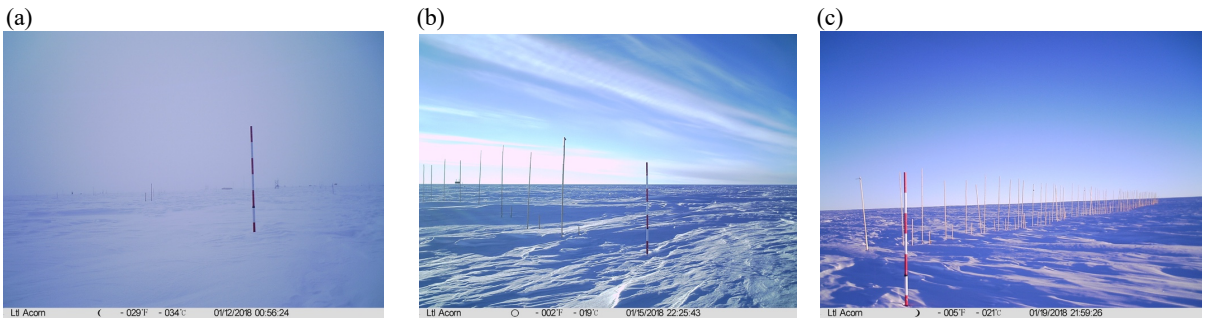

Figure 2. Examples of camera images. (a) #4 Dome Fuji, (b) #3 Relay point, (c) #2 Mizuho Station.

References

Motoyama, H., T. Furukawa, S. Fujita, K. Shinbori, Y. Tanaka, Y. Li, J. Chung, F. Nakazawa, K. Fukui, H. Enomoto, S. Sugiyama, H. Asano, Y. Takeda, M. Hirabayashi, D. Nishimura, T. Masunaga, T. Kuramoto, T. Kobashi, R. Kusaka, T. Kinase, C. Ikeda, T. Suzuki, H. Ohno, Y. Hoshina, Y. Hayakawa and T. Kameda, Glaciological data collected by the 48th–54th Japanese Antarctic Research Expeditions during 2007– 2013, JARE Data Rep. Glaciol., 341(35), 1– 44, 2015.

Sugiura, K., N. Hirasawa, N. Kurita, K. Kawamura, F. Nakazawa, H. Ohno, S. Fujita, I. Oyabu, T. Yamanouchi and H. Motoyama, Fixed point observation for daily snow surface monitoring along a latitudinal transect from the coast to the inland of Antarctica using camera images, The Tenth Symposium on Polar Science, OMp29, 2019.

Formation of layered firn within near-surface depths around Dome Fuji, East Antarctica from physical and chemical analyses of multiple firn cores

Ryo Inoue[1], Shuji Fujita[2,1], Kenji Kawamura[2,1,3], Motohiro Hirabayashi[2], Kumiko Goto-Azuma[2,1], Ikumi Oyabu[2], Fumio Nakazawa[2,1] and Hideaki Motoyama[2,1]

[1] *The Graduate University for Advanced Studies, SOKENDAI, Japan*

[2] *National Institute of Polar Research, Japan*

[3] *Japan Agency for Marine-Earth Science and Technology*

The physical and chemical properties of polar firn and their layerings initially formed or developed in the near-surface snow and affect the densification and bubble close-off process of firn (e.g., Hörhold and others, 2012; Fujita and others, 2016). Thus, it is important to better understand the formation of layered physical and chemical properties in near-surface firn. However, at low accumulation (< ~30 mm w.e. yr^{-1}) sites where deep coring is performed, there are little continuous and multi-property data (e.g., density, microstructure, water isotopes and impurities) from the same sample, partly because near-surface firn (at ~0–5 m) is often too fragile to collect in high quality. Hence, it is not well understood how density, microstructure, and their layering evolve with depth through temperature gradient metamorphism and how the layering of density and microstructure relates to the layering of chemical components. To solve these questions, we performed continuous and high-resolution (2.5–20-mm increment) analyses of multiple physical and chemical properties of firn cores and snow pit samples from seven sites around Dome Fuji (Table 1 and Figure 1). The properties include (1) density measured by a gamma-ray absorption method, (2) microwave permittivity ε as a proxy for density, (3) dielectric anisotropy Δε as a proxy for vertical elongation of ice and pore spaces, (4) near-infrared reflectance R as a proxy for specific surface area, and (5) $\delta^{18}O$, (6) Na concentration (5 and 6 are measured by a continuous flow analysis system). Here, we mainly focus on the top few meters of the samples. We found that, within the top ~3 m for all the measured samples, density increase tends to be smaller than that at deeper depths, Δε increases (more at lower accumulation sites), and SSA rapidly decreases. We also suggest that Δε increases preferentially in higher-density layers and the contrast between higher-density and lower-density layers is enhanced through temperature gradient metamorphism. In addition, we identified layers considering density, microstructure and chemical components together: (1) winter-spring layer preserving higher Na and lower $\delta^{18}O$ around Sep. – Nov., (2) Hard depth hoar with higher density, Δε and SSA, and (3) Skeleton-type depth hoar with lower density, Δε and SSA.

Sample name	Year of coring	Core length (m)	10 m snow temperature (°C)
S80	Jan. 2013	30	-
NDF18	Dec. 2017	152	-56.4
NDF13	Dec. 2012	31	-
NDFN	Dec. 2018	142	-
DFSE	Dec. 2017–Jan. 2018	41	-58.1
DFS	Dec. 2010	122	-
DF pit	Dec. 2007	3	-57.3
DFNW	Jan. 2018	43	-56.2

Table 1. Information of the samples.

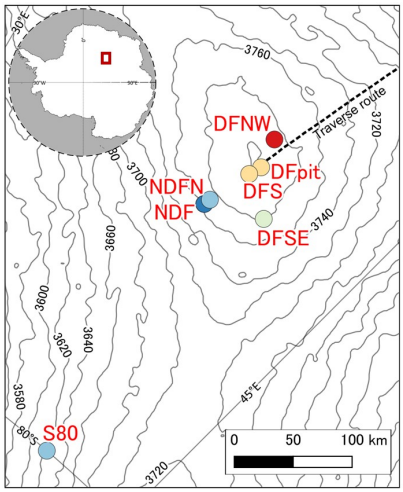

Figure 1. Locations of the sites where a firn core or snow block samples were collected.

References

Fujita S and others (2016) Densification of layered firn in the ice sheet at Dome Fuji, Antarctica. Journal of Glaciology 62(231).

Hörhold MW, Laepple T, Freitag J, Bigler M, Fischer H and Kipfstuhl S (2012) On the impact of impurities on the densification of polar firn. Earth and Planetary Science Letters 325–326, 93–99.

The Dome Fuji ice core DF2021 chronology (0 – 207 kyr BP)

Ikumi Oyabu[1], Kenji Kawamura[1,2,3], Christo Buizert[4], Frédéric Parrenin[5], Anais Orsi[6,7], Kyotato Kitamura[1], Shuji Aoki[8], Takakiyo Nakazawa[8]

[1] *National Institute of Polar Research, Japan*

[2] *The Graduate University of Advanced Studies (SOKENDAI), Japan*

[3] *Japan Agency for Marine Science and Technology (JAMSTEC), Japan*

[4] *Oregon State University, USA*

[5] *Université Grenoble Alpes, IGE, France*

[6] *Laboratoire des Sciences du Climat et de l'Environnement, LSCE/IPSL, CEA-CNRS-UVSQ, Université Paris-Saclay, France*

[7] *The University of British Columbia, Canada*

[8] *Tohoku University, Japan*

Precise ice-core chronologies are essential for identifying the timing and duration of polar climatic changes as well as their phasing with the changes in other parts of the globe. However, existing ice-core chronologies beyond the last 60 kyr show relatively large disagreements with each other and with U-Th chronologies of speleothems. Here, we constructed new ice and gas age scales for the Dome Fuji (DF) core (DF2021) over the last 207 kyr by combining a Bayesian dating model and firn densification model, constrained by various types of chronological and glaciological information including new $\delta O_2/N_2$ age markers, precise synchronization to other high-quality chronologies (volcanic, cosmogenic, and CH_4 signals), and high-resolution $\delta^{15}N$ of N_2 (reflecting past firn thickness). The new chronology is tightly constrained by synchronization to other well-dated records for the last 60 kyr, whereas it is independent from other chronologies for the older period. For the last 60 kyr, the DF2021 chronology agrees with the layer-counted ice core chronologies (GICC05 and a part of WD2014) and U-Th chronologies of speleothems within ~200 years. For the period 60 – 130 kyr BP, the timing of all Dansgaard-Oeschger warming events on DF2021 agree with those of corresponding events in the U-Th dated Chinese or European speleothems mostly within 1 kyr (well within 2σ uncertainty of DF2021). The excellent agreement suggests high accuracy of our chronology, and supports the assumption of negligible phasing between the past local summer solstice insolation and $\delta O_2/N_2$ fractionation at bubble close-off (the basis for constructing the $\delta O_2/N_2$ age markers). Between 130 and 207 kyr BP (penultimate glacial period), there is a lower degree of similarity between the variations in atmospheric CH_4 and speleothem calcite $\delta^{18}O$ than in the last glacial period, making the age comparison challenging. The comparison of DF2021 with 9 U-Th dates at 7 abrupt events shows the mean difference of -0.2 ± 0.8 kyr, which is within the DF2021 uncertainty (on the order of 1.5 kyr). The DF2021 chronology agrees with the AICC2012 chronology within 2 kyr except between ~103 and 128 kyr BP where AICC2012 is likely too young by up to ~4 kyr.

References

Oyabu, I., Kawamura, K., Buizert, C., Parrenin, F., Orsi, A., Kitamura, K., Aoki, S., and Nakazawa, T., The Dome Fuji ice core DF2021 chronology (0 – 207 kyr BP), *Quat. Sci. Rev.*, **294**, 2022, https://doi.org/10.1016/j.quascirev.2022.107754.

Changes in flux, size and composition of dust at Dome Fuji, Antarctica across Termination I

Kumiko Goto-Azuma[1,2], Motohiro Hirabayashi[1], Kaori Fukuda[1], Jun Ogata[1], Yoshimi Ogawa-Tsukagawa[1], Kyotaro Kitamura[1], Ayaka Yonekura[1,2,3], Shuji Fujita[1,2], Kenji Kawamura[1,2], Fumiko Nakazawa[1,2]

[1]*National Institute of Polar Research, Japan*
[2]*SOKENDAI (The Graduate University for Advanced Studies), Japan*
[3]*Present address: Marine Works Japan Ltd., Japan*

Mineral dust plays an important role in the climate system by affecting radiation budget, cloud microphysics, and atmospheric CO_2 concentration. In addition, dust responds to climatic changes. Therefore dust in paleoclimate archives can serve as excellent proxies for the past climate and environment. Dust in Antarctic deep ice cores have provided invaluable information on the past climatic and environmental changes in the southern hemisphere. However, due to very low concentrations in Antarctic ice cores, accurate and high-resolution continuous data have been limited. In particular, the information on changes in size and composition has been sparse. Here we present the results of accurate and high-resolution continuous analyses of dust concentrations, sizes, and compositions.

To study the dust variability from the Last Glacial Maximum (LGM) to mid-Holocene, we have analyzed the Dome Fuji deep ice-core using a Continuous Flow Analysis (CFA) system developed at the National Institute of Polar Research. With the CFA system, we measured microparticles, seven elements (Na, Mg, Al, Si, K, Ca, Fe and S), stable isotopes of water, black carbon and methane for the depth interval between 200 and 640 m. For accurate measurements of microparticle concentrations using a laser particle counter (Abakus, Markus Klotz), we improved the software. In addition to the CFA measurements, we collected discrete samples continuously at a 50 cm interval, and analyzed concentrations and size distributions using a Coulter counter (Multisizer 4, Beckman Coulter).

Abakus and Coulter counter data agreed well, and both particle counters could detect small changes in concentrations even during the Holocene when concentrations were low. The dust flux at Dome Fuji around the LGM was higher than that at Dome C (EDC) and lower than that at EDML (Kohnen), which reflects their distances from the major dust sources in South America. Dust size changes from the LGM to the Holocene at inland sites in East Antarctica have been reported to show regional differences (Delmonte et al., 2004; Wegner et al., 2012; Delmonte et al., 2017). At Dome Fuji, the dust size increased from the LGM to the Holocene, which is similar to EDC and EDML, but opposite to Dome B. By 16ka BP, the dust flux at Dome Fuji had decreased to the Holocene level, as was previously reported at other Antarctic deep core sites. Around that time, the relationship between dust size and dust concentration changed. Before that time, the dust size was almost constant, independent of dust concentrations, while after that time, dust size increased with dust concentration. Furthermore, the element compositions changed at that time. These results suggest that dust sources and/or transport pathways changed around 16ka BP.

References

Delmonte, B., J. R. Petit, K. K. Andersen, I. Basile-Doelsch, V. Maggi and V. Ya Lipenkov, Dust size evidence for opposite regional atmospheric circulation changes over east Antarctica during the last climatic transition, Climate Dynamics, 23, DOI: 10.1007/s00382-004-0450-9, 2004.

Wegner, A., P. Gabrielli, D. Wilhelms-Dick, U. Ruth, M. Kriews, P. De Deckker, et al., Change in dust variability in the Atlantic sector of Antarctica at the end of the last deglaciation, Climate of the Past, 8, 135-147, 2012.

Delmonte, B., C. I. Paleari, S. Andò, E. Garzanti, P. S. Andersson, J. R. Petit, et al. Causes of dust size variability in central East Antarctica (Dome B): Atmospheric transport from expanded South American sources during Marine Isotope Stage 2, Quaternary Science Reviews, 168, 55-68, 2017.

Variations in mineralogy of dust in ice cores obtained from northwestern and northeastern Greenland over the past 100 years

Naoko Nagatsuka[1], Kumiko Goto-Azuma[1, 2], Akane Tsushima[3], Koji Fujita[4], Sumito Matoba[5], Yukihiko Onuma[6], Yuki Komuro[7], Motohiro Hirabayashi[1], Jun Ogata[1], Yoshimi Ogawa-Tsukagawa[1], Kyotaro Kitamura[1], Teruo Aoki[1, 2], Trevor James Popp[8] and Dorthe Dahl-Jensen[8]

[1]*National Institute of Polar Research*

[2]*SOKENDAI*

[3]*Chiba University*

[4]*Nagoya University*

[5]*Institute of Low Temperature Science*

[6]*JAXA*

[7]*Laboratory for Environmental Research at Mount Fuji*

[8]*University of Copenhagen*

To reconstruct past variations in the sources and transportation processes of mineral dust in northwestern Greenland, we analysed the morphology and mineralogical composition of dust in the SIGMA-D ice core (77.64N, 59.12W, 2100 m a.s.l) from 1915 to 2013 using scanning electron microscope (SEM) and energy-dispersive X-ray spectroscopy (EDS). The results revealed the ice core dust consisted mainly of silicate minerals and that the composition varied substantially on multi-decadal and inter-decadal scales, suggesting that the ice core minerals originated from different geological sources in different periods during the past 100 years. The multi-decadal variation trend differed among mineral types. Kaolinite, which generally formed in warm and humid climatic zones, was abundant in colder periods (1950–2004), whereas mica, chlorite, feldspars, mafic minerals, and quartz, which formed in arid, high-latitude, and local areas, were abundant in warmer periods (1915–1949 and 2005–2013). Comparison of this information to Greenland surface temperature records indicates that this multi-decadal variation in the relative abundance of these different minerals was likely affected by local temperature changes in Greenland. Trajectory analysis shows that the minerals were transported mainly from its west coast during the two warming periods. This, in turn, was likely due to an increase in dust sourced from ice-free areas due to a shorter duration of snow and ice cover in Greenland's coastal region during the melt season caused by recent global warming. Meanwhile, ancient deposits in northern Canada, which were formed in past warmer climates, seem to be the best candidate during the colder period (1950–2004). Our results suggest that SEM–EDS analysis can detect variations in ice core dust sources during recent periods of low dust concentration (Nagatsuka et al., 2021).

To reveal spatial variation in the sources of minerals on the Greenland ice sheet, we have also analysed mineral dust from northeastern Greenland ice core (EGRIP: 75.62N, 35.96W, 2708 m a.s.l) during the past 100 years. The results showed the particle size, mineral composition, and compositional variations of the EGRIP ice core dust differed significantly than those of the SIGMA-D, indicating that the sources and transportation processes of the minerals were different between the two ice cores. The detailed discussion will be presented at the symposium.

References

Nagatsuka, N., Goto-Azuma, K., Tsushima, A., Fujita, K., Matoba, S., Onuma, Y., Dallmayr, R., Kadota, M., Hirabayashi, M., Ogata, J., Ogawa-Tsukagawa, Y., Kitamura, K., Minowa, M., Komuro, Y., Motoyama, H., and Aoki, T.: Variations in

mineralogy of dust in an ice core obtained from northwestern Greenland over the past 100 years, Clim. Past, 17, 1341–1362, 2021.

Snow accumulation inferred from a GPR survey around the Southeastern Dome, Greenland Ice Sheet

M. Minowa[1*], K. Fujita[2], S. Matoba[1] and Y. Iizuka[1]
[1]*Institute of Low Temperature Science, Hokkaido University, Japan*
[2]*Graduate School of Environmental Study, Nagoya University, Japan*

Snow accumulation is a component that is still poorly constrained over the Greenland Ice Sheet. We performed ground-penetrating radar (GPR) measurements around the Southeastern Dome (SE-Dome) of the Greenland Ice Sheet during a shallow ice core drilling campaign from May to June 2021 (Iizuka *et al*., 2021). GPR-derived firn structure was compared with ice core density, dates, and melt layers to reconstruct the snow accumulation around the SE-Dome. Numerous internal reflection horizons (IRHs) were observed, which were related to the ice core records (Fig. 1). We detected these IRHs automatically and calculated spatio-temporal snow accumulation rate around the SE-Dome. The calculated accumulation rates are ranged between 0.6 and 1.4 m w.e. a^{-1}, which agreed with previously reported snow accumulation at a neighboring ice core site (Furukawa *et al*., 2017). Although, the calculated snow accumulation varied not only in time but also in location. We discuss possible mechanisms of spatio-temporal variations in accumulation around SE-Dome at the conference.

References

[1] Iizuka, Y., *et al*. Glaciological and meteorological observations at the SE-Dome site, southeastern Greenland Ice Sheet. *Bul. Glaciol. Res.,* **34**, 2016
[2] Furukawa, R., *et al*. Seasonal-scale dating of a shallow ice core from Greenland using oxygen isotope matching between data and simulation. *J. Geophys. Res-Atmos.* **122**, 2017

Monitoring of polar snow for 20 years by satellite microwave observations

Riona Kasakawa[1], Hiroyuki Enomoto[1,2]
[1]*National Institute of Polar Research*
[2]*The Graduate University for Advanced Studies*

Cryospheric change due to accelerated warming in the Arctic is a major concern（ACIA, 2005）. Such a change influences the environment, resulting in atmospheric, oceanic, and terrestrial changes. Arctic research projects are sending field research groups and establishing observation sites at various places in this region. Satellite observations are available to support research planning, and evaluation of observation period and place, as these observations cover both time and space.

Observation of the melting of snow cover and ice sheets use of satellite microwave radiometers to detect moisture content in snow from microwave radiation. A method called XPGR (Cross-Polarization Gradient Ratio) has been used as a main observation algorithm since the late 1990s, and has been used in climate change research as an index of ice sheet melting. In addition, a method called Diurnal Amplitude variation (DAV) is used to observe the melting of snow cover on land. The advantages of DAV, which detects changes in surface snow, are that it is sensitive to short-term meteorological changes and captures short-term fluctuations (Alimasi, 2016). It is possible to conduct a comparative study of snow cover on land and on ice sheet. In this presentation, we examined the characteristics and precautions for using XPGR and DAV respectively. In addition, using meteorological reanalysis data, intercomparison with satellite observation, effectiveness of each method, and points to note were investigated. The data used are AMSR (2002-2011), AMSR-2 (2012-2021) and NCEP data for the same period. These methods can be applied across the polar regions.

Table 1.　Location of Arctic observation sites.

No.	Site	Lat.(degN)	Long.(degE)
	North America		
1	Resolute Bay	74.70	265.17
2	Cambridge Bay	69.20	255.55
3	Fort Smith	60.01	248.11
4	Inuvik	68.37	224.30
5	Barrow	71.30	203.41
6	Toolik Lake	68.63	210.40
7	Poker Flat	65.12	212.53
	Siberia		
8	Tiksi	71.00	127.00
9	Chokurdkha	70.00	148.00
10	Usti-Nera	64.57	143.24
11	Oymyakon	63.25	143.15
12	Suntar-Khayata	62.58	140.83
13	Spasskaya-Pad	62.23	129.62
14	Yakutsk	62.03	129.73
15	Ust-Maya	60.42	134.53
	Scandinavia/Svalbard		
16	Nortaustlandet	79.70	24.00
17	Ny-Ålesund	78.92	11.93
18	Kevo	69.75	27.02
19	Sodankylä	67.37	26.65

No.	Site	Lat.(degN)	Long.(degE)
	Greenland		
	Qaanaaq-NEEM Transect		
20	Qaanaaq (coast)	77.47	290.77
	ice sheet 400m	77.47	292.91
	ice sheet 1300m	77.57	297.24
～	ice sheet 1900m	77.48	299.56
	ice sheet 2000m	77.59	301.61
	ice sheet 2100m	77.47	303.90
21	NEEM Camp 2400m	77.45	308.40
	Lat. 67.5N Transect		
	glacier terminus 400m	67.50	310.00
	dark zone lower 1200m	67.50	311.00
	dark zone higher	67.50	311.50
	melt pond zone 1500m	67.50	312.00
22	ice/snow 1800m	67.50	313.00
	snow 2000m	67.50	314.00
	snow 2250m	67.55	315.29
	snow 2450m	67.54	316.45
	ridge 2500m	67.53	317.62

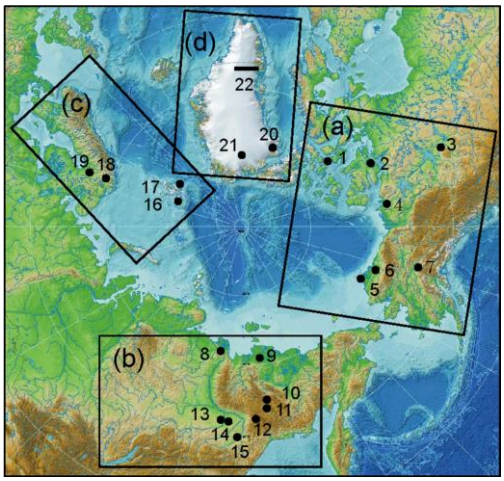

Figure 1.　Arctic observation sites .

References

Alimasi Nuerasimuguli，榎本浩之，2016, 衛星マイクロ波観測による北極域雪氷モニタリング―積雪期間と融雪期間の推定―．雪氷，79（1），17-30.

ACIA, 2005: Arctic Climate Impact Assessment, Cam　bridge University press, NY, 1042 pp.

Characteristics of cloud fraction and shortwave downward radiation at Syowa Station with ground-based observations

Yumi Shimode[1], Mana Takada[1], Amiri Yokotani[2], Makoto Kuji[3], Masanori Yabuki[4] and Naohiko Hirasawa[5,6]

[1]*Graduate School of Humanities and Sciences, Nara Women's University*

[2]*Faculty of Science, Nara Women's University*

[3]*Division of Natural Sciences, Faculty, Nara Women's University*

[4]*Research Institute for Sustainable Humanosphere, Kyoto University*

[5]*National Institute of Polar Research, Research Organization of Information and Systems*

[6]*Department of Polar Science, School of Multidisciplinary Sciences, SOKENDAI (The Graduate University for Advanced Studies)*

Cloud has warming and cooling effects on the Earth's climate: it absorbs earth radiation and reflects solar radiation, respectively. Their magnitudes depend on shape, height and amount of clouds, and so on. However, it is not easy to observe clouds precisely because of their spatial and temporal variability, e.g., wide variety of shapes and distributions. Cloud is one of the greatest sources of error in estimating radiative forcing and temperature in the future [IPCC 2013]. In addition, polar regions have a crucial impact on global climate through the existence of sea ice and ice sheet. Therefore, it is required to comprehend cloud behavior in polar regions.

In this study, we investigated the characteristics of three types of cloud fraction: all-sky camera, Micro Pulse LIDAR (MPL) and visual observations at Syowa Station, Antarctica. The all-sky camera continuously observes the whole sky every 10 min with a fisheye lens. We estimated cloud fraction from all-sky camera images based on a cloud detection method [Yabuki et al., 2014]. Using the all-sky camera, cloud has been detected only during the daytime period. MPL emits micro-pulse laser beams into the atmosphere and receives the backscattered light from cloud. Consequently, MPL can detect the presence of clouds, and thus, cloud fraction is estimated as the occurrence frequency. The visual cloud fraction was available from the Baseline Surface Radiation Network (BSRN). The visual observations are conducted every 3 h. We also investigated the relationship between these cloud fractions and shortwave downward radiation. The shortwave downward radiation observed by a pyranometer were also available every 1 min.

We investigated the variation of monthly-mean cloud fractions from all-sky camera, MPL and visual observations from 2005 to 2018. As a result, cloud fraction from the three observations generally showed similar variations. In addition, as a result of the correlation analysis of cloud fractions, all correlation coefficient is very high of 0.8 or higher. We are also going to discuss the results of correlation between cloud fractions and shortwave downward radiation.

Acknowledgments

The authors are grateful to those who devoted themselves to the observations. Cloud fraction with Eye observation and Shortwave downward radiation were provided from Baseline Surface Radiation Network (http://www.bsrn.awi.de/en/).

References

Intergovernmental Panel on Climate Change (IPCC2013), Climate Change 2013.

Yabuki, M., M. Shiobara, K. Nishinaka, and M. Kuji, Development of a cloud detection method from whole-sky color images, *Polar Science*, **8**, 315-326, 2014.

Comparison of cloud fractions from whole-sky camera observations around Syowa Station

Makoto Kuji[1], *Amiri Yokotani[2], Mana Takada[3], Yumi Shimode[3], Masanori Yabuki[4] and Naohiko Hirasawa[5,6]
[1]*Division of Natural Sciences, Faculty, Nara Women's University*
[2]*Faculty of Science, Nara Women's University*
[3]*Graduate School of Humanities and Sciences, Nara Women's University*
[4]*Research Institute for Sustainable Humanosphere, Kyoto University*
[5]*National Institute of Polar Research, Research Organization of Information and Systems*
[6]*Department of Polar Science, School of Multidisciplinary Sciences, SOKENDAI (The Graduate University for Advanced Studies)*

Cloud has opposite effects on the earth climate system: warming and cooling. Their magnitudes depend on cloud fraction, height, and so on. They influence the radiation balance on the earth and cloud is one of the greatest error sources for the climate prediction [IPCC, 2013]. Nevertheless, it is not easy to make a detailed observation due to their spatial and temporal variability. Furthermore, we do not have enough observation sites, especially over the ocean. Cloud has been observed by different instruments onboard R/V *Shirase* and at Syowa Station in Antarctica. By comparing these observations, we can confirm the consistency of the analysis methods of previous studies. Furthermore, it will allow us to elucidate cloud behavior in detail. In this study, we investigated cloud fractions around Syowa Station based on the whole-sky camera observations.

Shipboard observations were carried out onboard R/V *Shirase* (AGB-5003) [Kuji et al., 2016]. The whole-sky camera system mainly consists of a digital camera (NIKON D7000, NIKON Corporation) and a circular fisheye lens (4.5 mm F2.8 EX DC Circular Fisheye HSM, SIGMA Corporation) to take a photo of a whole sky. The observation interval is 5 min. We analyzed 14,688 images from 24 December 2017 to 12 February 2018 during the berth period of 59th Japanese Antarctic Research Expedition (JARE 59) around Syowa Station. We estimated cloud fraction from whole-sky camera images based on a cloud detection method [Yoshimura and Yamashita, 2013]. Furthermore, we analyzed the whole-sky images over sea ice region as a function of solar height because sea surface albedo over sea ice regions is very different from that over open ocean [Kuji et al., 2018]. Meanwhile, the whole-sky camera system (PSV-100, PREDE Corporation) installed at Syowa Station observes at 10 min intervals. We analyzed 4,230 images during the berth period of JARE 59. From these whole-sky color images, we estimated cloud fraction based on the cloud detection method [Yabuki et al., 2014].

We investigated the temporal variation of the cloud fractions from the whole-sky camera observations during the berth period of JARE 59. As a result, it is found that the variation of cloud fractions is generally consistent and the correlation coefficient is very high of 0.93.

Furthermore, we are going to compare the cloud fractions estimated from the whole-sky camera during JARE55 to 61 as a whole and discuss the characteristics of the cloud fractions around Syowa Station.

Acknowledgments

The shipborne whole-sky camera observations were conducted in cooperation with Japan Aerospace Exploration Agency (JAXA) and National Institute of Polar Research. The authors are grateful to those who related to observations at Syowa Station and onboard R/V *Shirase* during JARE 55-61.

References

Intergovernmental Panel on Climate Change (IPCC2013), Climate Change 2013.

Kuji, M., R. Fujimoto, M. Miyagawa, R. Funada, M. Hori, H. Kobayashi, S. Koga, J. Matsushita, and M. Shiobara, Cloud fractions estimated from shipboard whole-sky camera and ceilometer observations, *Transactions of the Japan Society for Aeronautical and Space Sciences*, **14**, 7-13, 2016.

Kuji, M., A. Murasaki, M. Hori, and M. Shiobara, Cloud Fractions Estimated from Shipboard Whole-sky Camera and Ceilometer Observations between East Asia and Antarctica. *J. Meteor. Soc. Japan*, **96**, 201-214, 2018.

Yabuki, M., M. Shiobara, K. Nishinaka, and M. Kuji, Development of a cloud detection method from whole-sky color images, *Polar Science*, **8**, 315-326, 2014.

Yoshimura, M. and M. Yamashita, Contribution of Ground-Based Cloud Observation to Satellite-Based Cloud Discrimination, *J. Environ. Sci. Eng*. A, **2**, 379-382, 2013.

4-year (2018-2021) variations of river surface temperature and channel width in the Arctic region derived from GCOM-C/SGLI

Masahiro Hori[1]
[1]*University of Toyama*

The Arctic rivers play important roles in the continental hydrological cycles as well as the ocean-atmosphere energy exchange in the Arctic (Park et al., 2020). Recently, the snow cover extent in the Northern Hemisphere has been declining during the past 40 years (Hori et al., 2017). Thus, the temporal pattern of fresh water and heat inflow into the Arctic Ocean through the continental rivers can be considered to change drastically. This study aims to derive river surface temperature and channel width of the six Arctic rivers (Ob, Yenisei, Lena, Kolyma, Yukon, and Mackenzie) from remotely sensed images using optical sensor SGLI onboard GCOM-C satellite launched in 2017. SGLI has spectral channels in the visible to thermal infrared wavelength regions at the spatial resolution of 250 m, which enables us to monitor river surface temperature (RST) and river channel width (RCW) on the continental scale. Analysis of the first two-year SGLI data (2018-2019) revealed that RST and RCW can be retrieved successfully on a near-daily basis (Hori, 2021). In this study, the period of data analysis was extended to four years from 2018 to 2021 in order to capture seasonal and yearly changes in RST and RCW. Figure 1 indicates daily anomalies of RST and RCW along the Lena River from 2018 to 2021. SGLI-derived RST and RCW varies coincidently. That is, when RST becomes lower, RCW tends to be wider, and vice versa. This can be considered due to that the occurrence of precipitation within river basins leads to the increase of river discharge (i.e., RCW) together with the decrease of RST, because cloudy condition reduces the temperature of land surface on which surface runoff flows into the river channel. The amplitude of RST and RCW variations also varies year by year. Thus, heat flux flowing into the Arctic Ocean through the Lena River is also considered to vary year by year and could affect sea surface temperature and sea ice distribution in the Arctic Ocean.

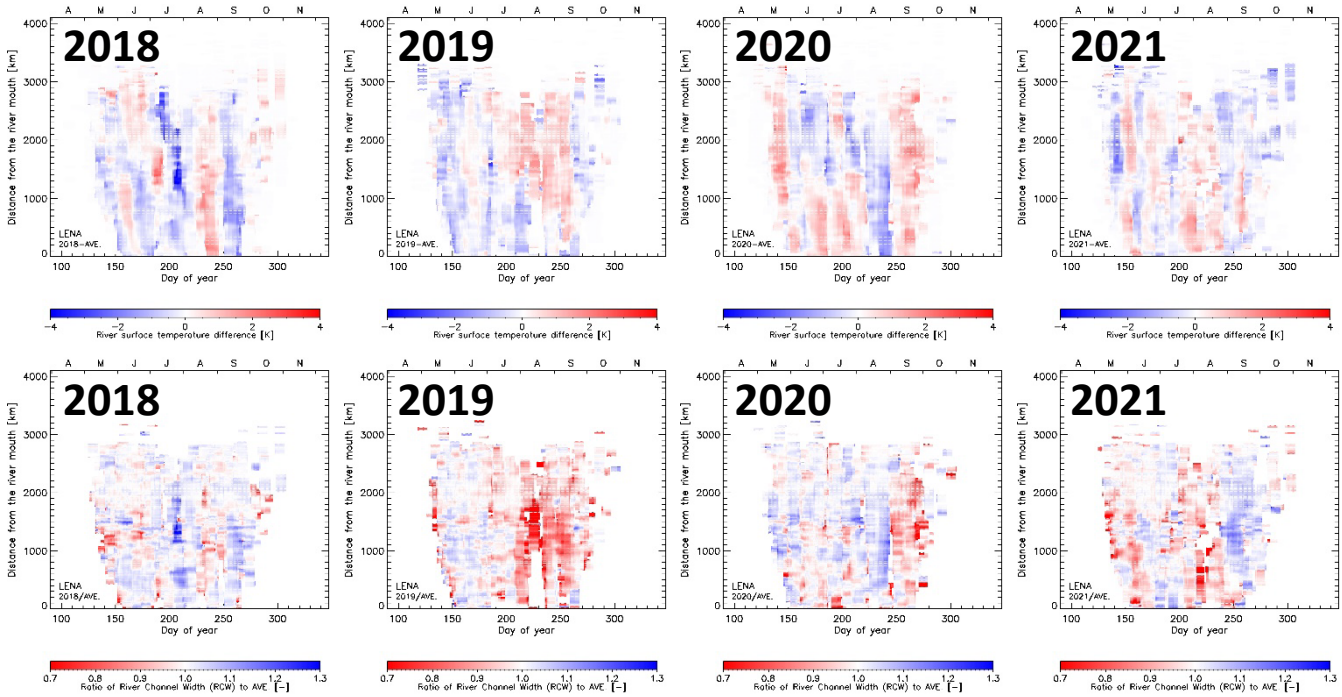

Figure 1 Spatio-temporal distribution of SGLI-derived river surface temperature (RST, upper figures showing as anomalies from 4-year average) and river channel width (RCW, lower figures as the ratio to 4-year average) along the Lena River channel from 2018 to 2021.

References

Hori, M., Near-daily monitoring of surface temperature and channel width of the six largest Arctic rivers from space using GCOM-C/SGLI. Remote Sens. Environ., 263, 112538. doi: 10.1016/j.rse.2021.112538, 2021.

Hori, M., K. Sugiura, K. Kobayashi, T. Aoki, T. Tanikawa, K. Kuchiki, M. Niwano and H. Enomoto, A 38-year (1978–2015) Northern Hemisphere daily snow cover extent product derived using consistent objective criteria from satellite-borne optical sensors, Remote Sensing of Environment, 191, 402-418, https://doi.org/10.1016/j.rse.2017.01.023, 2017.

Park, H., Watanabe, E., Kim, Y., Polyakov, I., Oshima, K., Zhang, X., Kimball, J.S., Yang, D., 2020. Increasing riverine heat influx triggers Arctic sea ice decline and oceanic and atmospheric warming. Sci. Adv. 6 (45), eabc4699, 2020.

A hemispheric extreme warm winter in 2019-20 enhanced by the highest sea surface temperature around mid-latitude

Yuta Ando[1, 2], and Yoshihiro Tachibana[3]
[1]*Graduate school of Science and Technology, Niigata University*
[2]*National Institute of Technology, Suzuka College*
[3]*Weather and Climate Dynamics Division, Mie University*

In 2020 winter, most mid latitudes in the Northern Hemisphere was the historically warmest (Fig. 1a). The warmth was spreading zonally around all the mid latitudes throughout the season. Zonal-mean sea surface temperature in the mid latitudes was also unprecedently warm (Fig. 1b). It was substantially different from the recent localized extreme weathers, which were smaller both in temporal and spatial scales than 2020. The global warming might have turned into reality. Here we show that synchronized chain interaction between the warm seas and the warm atmosphere amplified the anomalousness of the warm winter using data analyses and simple numerical experiments. The chain is as follows; the warm seas built up in the previous autumn made overlying air warm, then the warmed air penetrated inland by westerlies, the warm air over the land further flew to the ocean, which again warms the seas. The zonal oceanic warming in mid-latitudes might shift the climate dynamics to a new state. This air-sea chain was responsible for unprecedently positive phase of Arctic Oscillation, which is a good measure of the zonal mean extreme warmth.

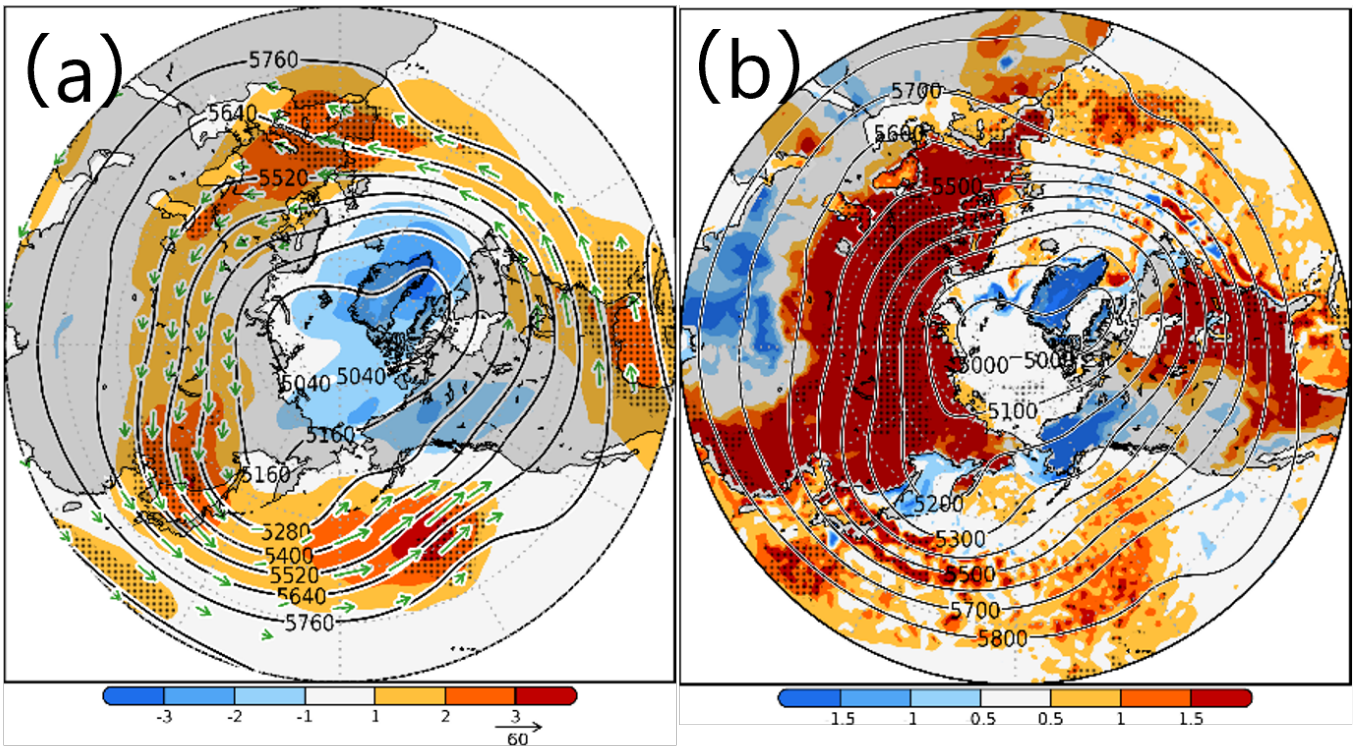

Figure 1 **(a)** Three-month mean air temperature anomalies (color shading [K], hatch: recorded the highest since 1979) at 500 hPa, and geopotential height (contours [m]) at 500hPa in winter 2020 between 1 January and 31 March. **(b)** same as Fig. 1a, but sea surface temperatures (ocean area) and ground temperature (land area).

Seasonal variations of the partial pressure of CO_2 in surface water and quantitative assessment of its drivers in the Pacific Sector of the Arctic Ocean from winter to summer

Manami Tozawa[1], Daiki Nomura[1,2,3], Mariko Hatta[4], Amane Fujiwara[4], Sayaka Yasunaka[5], Akihiko Murata[4]

[1]*Faculty/Graduate School of Fisheries Sciences, Hokkaido University,*

[2]*Field Science Center for Northern Biosphere, Hokkaido University,*

[3]*Arctic Research Center, Hokkaido University,*

[4]*Japan Agency for Marine-Earth Science and Technology (JAMSTEC),*

[5]*Graduate School of Science, Tohoku University*

To comprehend the variations in the partial pressure of CO_2 (pCO_2) in the surface water in the Arctic Ocean and to identify its drivers, we conducted biogeochemical observation in the Pacific Sector from September to October 2021. The pCO_2 in surface water was undersaturated with respect to the atmosphere, indicating a CO_2 sink for the atmosphere in the study area. We estimated the surface water pCO_2 under sea ice in winter to be 363±14 µatm based on the water temperature, dissolved inorganic carbon, and total alkalinity at the winter water layer (175−220 m). Then, we also evaluated the variations of pCO_2 (δpCO_2) by temperature, freshwater inflow, and biological activity to assess the drivers determining pCO_2 quantitatively from winter to summer. In the area south of 70˚N, although a dramatical increase of the sea surface temperature from winter toward summer had the potential to increase pCO_2 and then should have led to the CO_2 supersaturation with respect to the atmosphere, the freshwater inflow and the biological activity reduced the pCO_2, and led the CO_2 undersaturation with respect to the atmosphere. In the northern part of the observation area (>72˚N), pCO_2 was lower than the value in the atmosphere due to a slight seasonal variation in sea surface temperature and significant freshwater inflow reducing pCO_2 in surface water as the result of the dilution effect. Furthermore, the freshwater origins (sea ice meltwater and snow meltwater) were identified using stable oxygen isotopic ratio and salinity, and it suggested that the impact on pCO_2 would vary depending on the freshwater source.

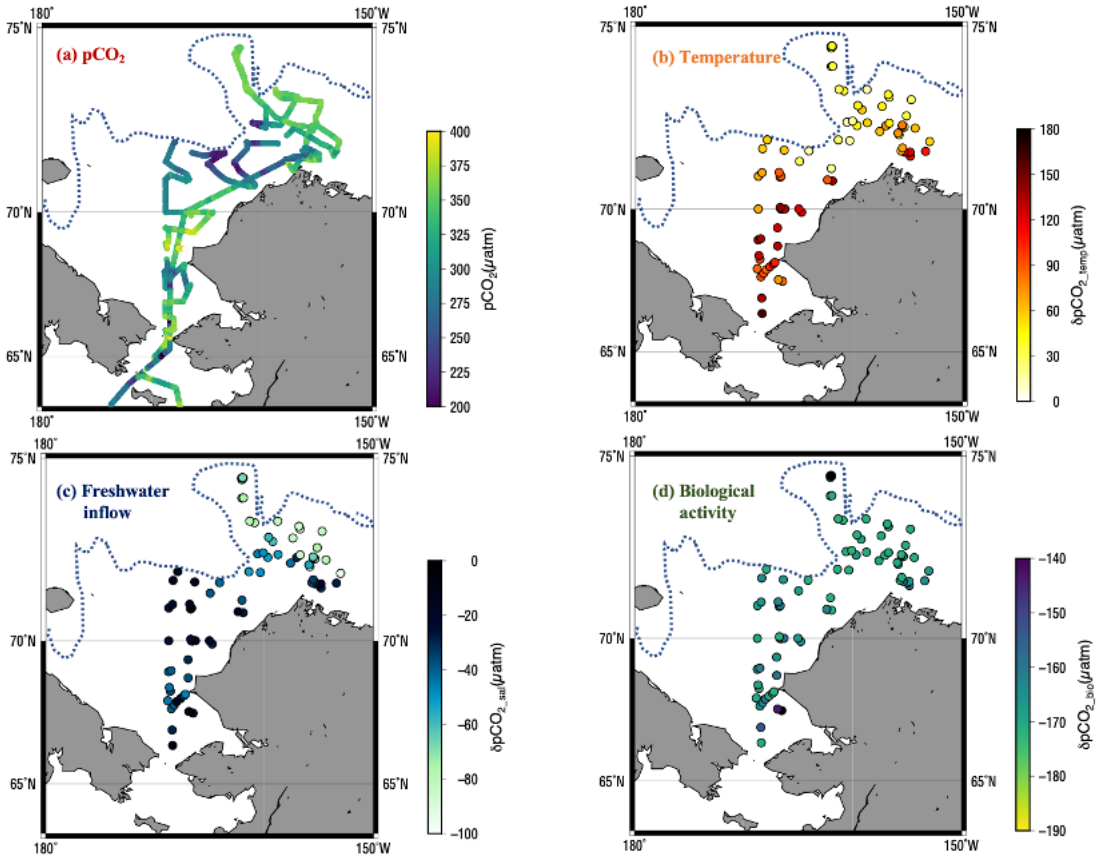

Figure 1. (a) Spatial distribution of pCO_2 in summer, (b) δpCO_2 by temperature, (c) δpCO_2 by freshwater inflow, and (d) δpCO_2 by biological activity

Global distribution of decoupling between silicate and nitrate in the ocean

Pan XL [1], Lai XX [1], Li BF [2] and Watanabe YW [2]

[1] *Graduate School of Environmental Earth Science, Hokkaido University, Japan*
[2] *Faculty of Environmental Earth Science, Hokkaido University, Japan*

The biological productivity of the ocean has a significant impact on controlling atmospheric CO_2 level. The surface layer of the Southern Ocean (SO) serves as the major source of nutrients for primary production in global low-latitude surface waters with the formation of the Intermediate Water (IW) *[Sarmiento et al., 2004; Palter et al., 2010]*. The high downward export flux of biogenic silica from the surface SO results in a much greater decrease gradient of dissolved silica (Si) which decoupled from that of nitrate (N) along the northward transportation of IW, thus limiting biological productivity in most of the global surface ocean. Due to the sparseness of extensive time-series observation of nutrients across the global ocean, especially in the SO, such decoupling between Si and N is still understood in a very vague way. Recently, parameterization technique has proven to be a good solution to the problem of insufficient ocean observation *[Pan et al., 2020; Pan et al., 2022]*. Here we attempt to quantify the seasonal downward export fluxes of Si and N from surface as well as the upward resupply fluxes by using neural network parameterizations and biogeochemical Argo float (BGC-Argo), and to directly estimate this decoupling between Si and N over the global surface ocean. We found a contrast downward export ratio of Si and N (Si/N) between the SO of 8:1 and the North Atlantic of 0.1:1. IW-derived water masses with Si/N ≥ 1 are found in the major global upwelling regions, such as the equatorial Pacific and the Subarctic Pacific. Lower Si/N in these regions (~2:1) than that in the SO is probably due to the deficiency of Si or the supply of terrestrial-origin iron. The imbalance between the downward export and the upward resupply allows us to identify the main regions of Si removal from the surface that result in the meridional descending gradient of Si in the global ocean. Our results have important implications for our understanding of the nutrient dynamics of the global surface ocean and future climate change.

References

Sarmiento, J., Gruber, N., Brzezinski, M. A., and Dunne, J. P.: High-latitude controls of thermocline nutrients and low latitude biological productivity, *Nature*, 427, 56–60 (2004)

Palter, J. B., Sarmiento, J. L., Gnanadesikan, A., Simeon, J., and Slater, R. D.: Fueling export production: nutrient return pathways from the deep ocean and their dependence on the Meridional Overturning Circulation, *Biogeosciences*, 7, 3549–3568 (2010)

Pan, X. L., Li, B. F. & Watanabe, Y. W. The Southern Ocean with the largest uptake of anthropogenic nitrogen into the ocean interior. *Sci. Rep.* **10**, 8838, (2020)

Pan, X. L., Li, B. F. & Watanabe, Y. W. Intense ocean freshening from melting glacier around the Antarctica during early 21st century. *Sci. Rep.* **12**, 1–10 (2022)

Sea Ice Thickness Measurement Using UAV-SfM

Yuki Ouchi[1], Kazutaka Tateyama[2], Tatsuya Watanabe[2], Kohei Sato[3], Takuji Waseda[4,5],
Tsubasa Kodaira[5], Ryosuke Uchiyama[5]

[1] *Graduate School of Engineering, Kitami Institute of Technology, Kitami, Japan*

[2] *School of Earth, Energy and Environmental Engineering, Kitami Institute of Technology, Kitami, Japan*

[3] *Civil Engineering Research Institute for Cold Region, Sapporo, Japan*

[4] *Japan Agency for Marine-Earth Science and Technology(JAMSTEC), Yokohama, Japan*

[5]*Graduate School of Frontier Sciences, The University of Tokyo, Kashiwa, Japan*

Sea ice thickness is important information for elucidating the effects of climate change and for economic activities in ice covered sea area. Declining sea ice has potential for Northern Sea Route（NSR) and resource exploitation. Therefore, it is necessary to understand not only the extent but also the thickness and surface condition of sea ice. Conventional methods for measuring sea ice thickness such as a drill-hole method have some weakness points like high labor and inefficiency. An Unmanned Aerial Vehicle with Structure from Motion (UAV-SfM) is applied for sea ice thickness measurement in order to achieve low cost, high efficiency, and accurate observation over a wide area under low temperature conditions.

Observations of snow and ice surfaces heights by UAV-SfM have been conducted most on the lake ice of the Saroma-ko Lagoon and the land-fast sea ice near the coast. In this study, aerial photographs of sea ice were taken by UAV “DJI Phantom4-pro” and the photographs were analyzed by SfM software “Metashape”. In addition, A Global Navigation Satellite System (GNSS) receiver was mounted on the UAV to get coordinates of each aerial photograph. Figure 1 shows the location and the observation area of the Utoro port of eastern Hokkaido, Japan. The observation date is on February 12, 2022. Ice cake existed in the port on that day (Figure 2). The flight time was from 9:36 a.m. to 10:56 a.m. We got 414 photographs by three flights (approximately 20 minutes each). We measured sea ice thickness at 10 points by a drill-hole method to compare actual and estimated values. The Digital Surface Model (DSM) of sea ice surface height was generated from the SfM software. Freeboard and thickness of sea ice were estimated from the DSM and hydrostatic equilibrium. Figure 3 shows the estimated freeboard distribution in the observation area (Fig. 1). Mean Absolute Error (MAE) and Root Mean Squared Error (RMSE) between actual and estimated values were 2.3cm and 2.8cm. The estimated ice thickness was also compared with the results of sea ice measurements by sea ice / wave radar.

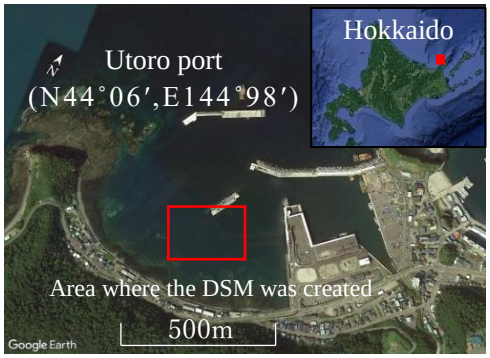

Figure 1. The location and observation area

Figure 2. Ice conditions in Utoro port

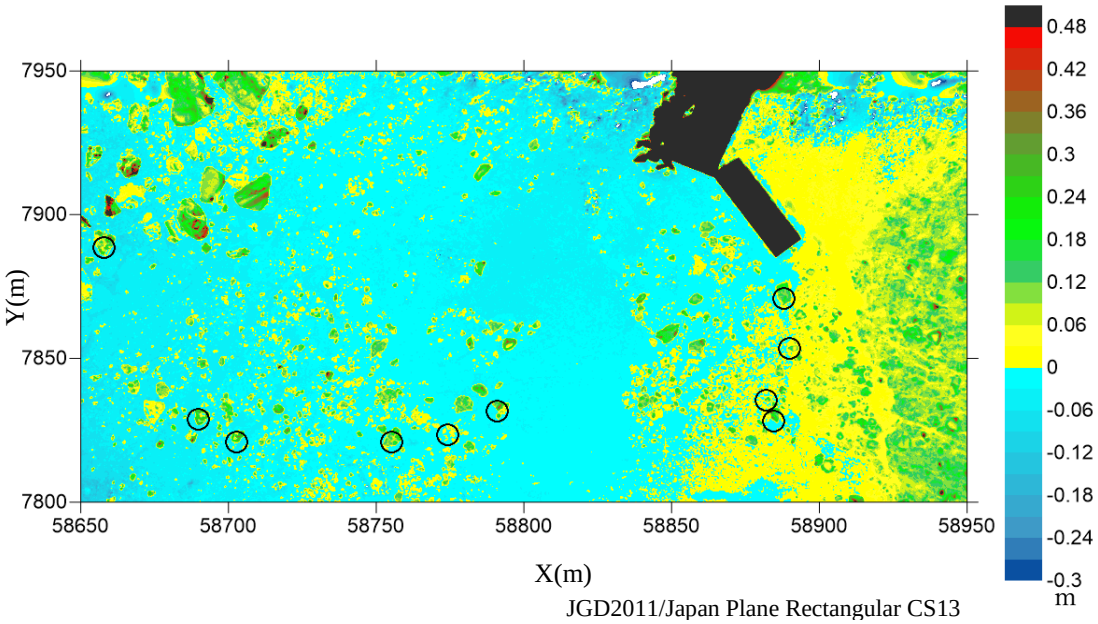

○：drilling locations

Figure 3. Spatial distribution of freeboard in the area of red square in Fig.1.

References

Watanabe, T., Tateyama, K: An attempt to measure sea ice freeboard using UAV-SfM, Seppyo, **83**(2), 155-167, 2021.

Sato, K., Tateyama, K., Watanabe, T., Tanikawa T: Observation of Total Ice Thickness Using UAV-SfM in the Saroma-ko Lagoon, The 12th Symposium on Polar Science, online, November, 2021.

Lagged effect of tropical ocean on sea ice variability in the Sea of Okhotsk

Mitsuki Takehata[1], Yoshihiro Tachibana[1], and Yuta Ando[2, 3]
[1]*Weather and Climate Dynamics Division, Mie University*
[2]*Graduate School of Science and Technology, Niigata University*
[3]*National Institute of Technology, Suzuka College*

The Sea of Okhotsk is a unique sea, where sea ice spreads to the lowest latitudes in the world. Sea ice extent in the Sea of Okhotsk varies remarkably from year to year controlled by various factors. One of the important factors is a remote effect. Previous studies showed that the sea ice extent in the Sea of Okhotsk increased in years of El Niño events, however, the lagged effect from the tropical ocean has not been considered. Tropical ocean has the significant-lagged impact on other regions such as the tropical Indian Ocean (TIO) capacitor effect (Xia et al., 2009). The TIO capacitor effect is a phenomenon in which the influence of the tropical Pacific Ocean appears in the TIO with a lag of 2-3 months. We therefore examined the lagged relationship between the tropical ocean and sea ice variability in the Sea of Okhotsk using statistical analysis. We found that sea ice extent in the Sea of Okhotsk was increased in the next winter after the La Niña events (Fig. 1a). We suggest the hypotheses that a process of relationship between La Niña and the variability of the sea ice extent in the Sea of Okhotsk in next winter are as follows: 1) In the La Niña winter, anomalous convection near the Philippine Sea persisted until half a year later in the summer. 2) Anomalous convection excites the Pacific-Japan teleconnection pattern, which are related to low pressure anomalies near Siberia (Fig. 1b) and low temperature anomalies in the soil. 3) The low temperature anomalies in the soil around Siberia persist until early winter, bringing cold air to the Sea of Okhotsk and increasing sea ice. Some of these process were also confirmed by numerical model experiments.

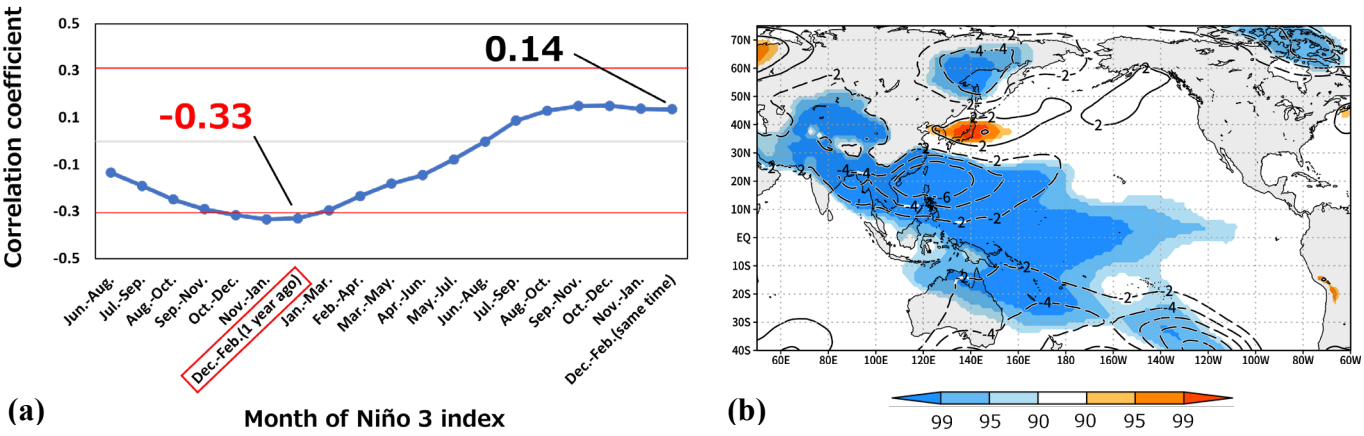

Figure 1. **(a)** Time series of lagged correlation coefficients between the Sea of Okhotsk sea ice extent and the Niño 3 indices. The red line indicates a confidence level of 95%. **(b)** Regression between the three months averaged OLR index in the Philippine Sea from June to August with the geopotential height of 850 hPa in the same time. Contours indicate regression coefficients (m). Color shading indicates confidence levels.

Reference

Xie, S.-P. et al. 2009：Indian Ocean Capacitor Effect on Indo–Western Pacific Climate during the Summer following El Niño. *Journal of Climate*, **22(3)**, 730-747.

Seasonal and interannual changes in the lake surface of Izunuma wetland

Tatsuru Sato
Ichinoseki Collage, National Institute of Technology

Internet of Things (IoT) technology has been developed to utilize information by connecting various devices to a network. These technologies are capable of collecting and analyzing environmental information in remote and inaccessible areas, and are important for obtaining real-world information in situations where mobility is restricted. The Izunuma and Uchinuma wetland areas located in the northern part of Miyagi Prefecture in the Tohoku region are internationally important wetlands and have been registered under the Ramsar Convention. Japanese Ministry of the Environment has established the Internet Nature Research Center (2021), which connects images taken in nature parks by camera to a network in an attempt to utilize them for nature park management and information disclosure. Every winter, 100,000 migratory birds fly to Izunuma from the Arctic region of Siberia to overwinter around the lake. In this study, these images were used to analyze the winter environment of the lake and to obtain vegetation information during the summer season.

A study of changes in the number of days of lake surface freezing shows that even in the early 2010s, the number of days of freezing in winter (DJF) ranges from 10 to 40 days. The number of days of freezing is high and low every few years, and the number of days of freezing is particularly high in the years of low temperatures and heavy snowfall in northern Japan. In the analysis of the camera images so far, it is found that the number of freezing days in the winter season of 2020 (December 2020 to February 2021) is the largest (48 days), and that in 2019 it is the smallest. Classification of the lake surface was conducted using image data from spring and summer using a neural network to discriminate the vegetation of the lotus, and it was found that the classification was highly accurate (approximately 98%), indicating that discrimination by the presence of vegetation is possible. Therefore, we prepared a cutout of the lake surface from the images from 2013 to 2017 and calculated the percentage of green to the entire lake surface using HSV. The the highest percentage of vegetation was found around August each year, and that within a few weeks, the vegetation took up the majority of the lake surface. The weather data for the points where the percentage of green vegetation decreased dramatically showed a significant increase in precipitation (e.g. typhoon).